Mapping high-resolution soil moisture and properties using distributed temperature sensing data and an adaptive particle batch smoother

Dong, Jianzhi; Steele-Dunne, Susan C.; Ochsner, Tyson E.; Hatch, Christine E.; Sayde, Chadi; Selker, John; Tyler, Scott; Cosh, Michael H.; van de Giesen, Nick

DOI
10.1002/2016WR019031

Publication date
2016

Document Version
Final published version

Published in
Water Resources Research

Citation (APA)
Dong, J., Steele-Dunne, S. C., Ochsner, T. E., Hatch, C. E., Sayde, C., Selker, J., Tyler, S., Cosh, M. H., & van de Giesen, N. (2016). Mapping high-resolution soil moisture and properties using distributed temperature sensing data and an adaptive particle batch smoother. *Water Resources Research*, *52*(10), 7690-7710. https://doi.org/10.1002/2016WR019031

AGU PUBLICATIONS

Water Resources Research

RESEARCH ARTICLE
10.1002/2016WR019031

Key Points:
- A new data assimilation approach, the Adaptive Particle Batch Smoother, is presented
- APBS can estimate soil moisture and soil properties using soil temperatures
- APBS was applied to distributed temperature sensing observations to yield meter resolution soil moisture

Correspondence to:
J. Dong,
j.dong-1@tudelft.nl

Citation:
Dong, J., S. C. Steele-Dunne, T. E. Ochsner, C. E. Hatch, C. Sayde, J. Selker, S. Tyler, M. H. Cosh, and N. van de Giesen (2016), Mapping high-resolution soil moisture and properties using distributed temperature sensing data and an adaptive particle batch smoother, *Water Resour. Res.*, *52*, 7690–7710, doi:10.1002/2016WR019031.

Received 6 APR 2016
Accepted 18 SEP 2016
Accepted article online 21 SEP 2016
Published online 6 OCT 2016

Mapping high-resolution soil moisture and properties using distributed temperature sensing data and an adaptive particle batch smoother

Jianzhi Dong[1], Susan C. Steele-Dunne[1], Tyson E. Ochsner[2], Christine E. Hatch[3], Chadi Sayde[4], John Selker[4], Scott Tyler[5], Michael H. Cosh[6], and Nick van de Giesen[1]

[1]Water Resources Section, Faculty of Civil Engineering and Geosciences, Delft University of Technology, Delft, Netherlands, [2]Department of Plant and Soil Sciences, Oklahoma State University, Stillwater, Oklahoma, USA, [3]Geosciences Department, University of Massachusetts, Amherst, Massachusetts, USA, [4]Department of Biological and Ecological Engineering, Oregon State University, Corvallis, Oregon, USA, [5]Department of Geological Sciences and Engineering, University of Nevada, Reno, Reno, Nevada, USA, [6]Hydrology and Remote Sensing Laboratory, U.S. Department of Agriculture, Agricultural Research Service, Beltsville, Maryland, USA

Abstract This study demonstrated a new method for mapping high-resolution (spatial: 1 m, and temporal: 1 h) soil moisture by assimilating distributed temperature sensing (DTS) observed soil temperatures at intermediate scales. In order to provide robust soil moisture and property estimates, we first proposed an adaptive particle batch smoother algorithm (APBS). In the APBS, a tuning factor, which can avoid severe particle weight degeneration, is automatically determined by maximizing the reliability of the soil temperature estimates of each batch window. A multiple truth synthetic test was used to demonstrate the APBS can robustly estimate soil moisture and properties using observed soil temperatures at two shallow depths. The APBS algorithm was then applied to DTS data along a 71 m transect, yielding an hourly soil moisture map with meter resolution. Results show the APBS can draw the prior guessed soil hydraulic and thermal properties significantly closer to the field measured reference values. The improved soil properties in turn remove the soil moisture biases between the prior guessed and reference soil moisture, which was particularly noticeable at depth above 20 cm. This high-resolution soil moisture map demonstrates the potential of characterizing soil moisture temporal and spatial variability and reflects patterns consistent with previous studies conducted using intensive point scale soil moisture samples. The intermediate scale high spatial resolution soil moisture information derived from the DTS may facilitate remote sensing soil moisture product calibration and validation. In addition, the APBS algorithm proposed in this study would also be applicable to general hydrological data assimilation problems for robust model state and parameter estimation.

1. Introduction

Remote sensing observed soil moisture products are essential for our understanding of climatic and hydrological processes [*Seneviratne et al.*, 2010; *Koster et al.*, 2003; *Taylor et al.*, 2012] and improving modeling skills [*Crow and Ryu*, 2009; *Chen et al.*, 2011; *Koster et al.*, 2010; *Hazenberg et al.*, 2015; *Niu et al.*, 2014; *Wood et al.*, 2011]. However, validating remote sensing products and downscaling coarse resolution products to model scales are both necessary and challenging [*Crow et al.*, 2012; *Famiglietti et al.*, 2008]. This is because mapping the soil moisture field using intensively collected point-scale soil moisture samples, or dense networks of point scale soil moisture sensors is usually logistically infeasible [*Steele-Dunne et al.*, 2010]. Innovative techniques proposed in recent years, e.g., cosmic-ray neutron probe [*Zreda et al.*, 2008] and GPS interferometric reflectometry [*Larson et al.*, 2008], can provide areal mean soil moisture values over an area with a diameter of a few hundred meters. However, these techniques cannot provide soil moisture spatial variability information within the measurement area.

Distributed Temperature Sensing (DTS) has the potential to provide unique insights into the link between soil moisture observations at meter to intermediate and footprint scales [*Ochsner et al.*, 2013]. This may substantially improve our knowledge of soil moisture scaling and footprint-scale soil moisture validation. DTS measures environmental temperature with a spatial resolution less than 1 m and temporal resolution less

than 1 min [*Selker et al*., 2006]. Soil thermal properties are a function of soil moisture, and hence the soil heat transfer process can be monitored to estimate soil moisture. One category of DTS methods is called active DTS, in which electrically generated heat pulses are used. Soil temperature change due to these heat pulses can be used to estimate soil moisture using either empirically calibrated or physically based equations [*Sayde et al*., 2010; *Ciocca et al*., 2012; *Striegl et al*., 2012]. Active DTS is relatively accurate, especially at low soil moisture contents [*Sayde et al*., 2010; *Ciocca et al*., 2012; *Striegl et al*., 2012]. However, the large power requirement for generating heat pulses can be a logistical obstacle for field implementations. Further, the active DTS method is also sensitive to any air gaps between the DTS cable and the soil [*Sourbeer and Loheide*, 2015]. Passive DTS estimates soil moisture only using naturally occurring soil temperatures. In an early passive DTS study [*Steele-Dunne et al*., 2010], soil temperatures measured at three depths were used to estimate soil thermal diffusivity. Soil moisture could then be inferred, provided the relationship between soil thermal diffusivity and soil moisture relationship was known. The passive DTS method overcomes several challenges in the active DTS method, but it also has several limitations. First, soil thermal diffusivity is insensitive to soil moisture for a wide range of soil moisture values. Second, physically reasonable estimates cannot be obtained from the inversion approach of *Steele-Dunne et al*. [2010] when solar radiation is low. Third, it is difficult to determine the soil thermal diffusivity to moisture relationship along the cable, when the spatial variability of soil properties is high. Finally, the passive DTS method is very sensitive to uncertainty in cable depths.

Dong et al. [2015a] tackled the first two of these challenges using data assimilation. In their study, a fully coupled soil water, heat and vapor transfer model (Hydrus-1D) [*Simunek et al*., 2009] was used to provide so-called a priori soil moisture and temperature profiles. Soil temperature observed at two depths (5 and 10 cm) were sequentially assimilated using the ensemble Kalman filter (EnKF) [*Evensen*, 2003] to update the prior guessed soil temperature and moisture profile.

In a subsequent study, a particle batch smoother (PBS) was used by *Dong et al*. [2015b] to estimate soil moisture using series of soil temperature observations. The evolution of the soil temperature within a certain time window may contain more information on soil moisture, since the rates of heating and cooling may be better observed. Thus, a batch smoothing technique is more suitable, i.e., using all the soil temperature observations within a certain period of time (batch window) to update the soil moisture estimates within this window. The Ensemble Smoother (ES) [*Van Leeuwen and Evensen*, 1996] assumes the prior distribution is normally distributed, and hence the ES may provide inaccurate estimates when the prior distribution is highly non-Gaussian [*Van Leeuwen and Evensen*, 1996]. The "particle" approach, in which the entire distribution is mapped using Monte Carlo sampling points, has been shown to be superior to ensemble techniques when the Gaussian assumption is violated, and particle approaches are particularly effective in parameter estimation [*Dechant and Moradkhani*, 2011; *DeChant and Moradkhani*, 2012; *Moradkhani et al*., 2012]. In a follow-up study, *Dong et al*. [2016a] used synthetic tests to show that soil moisture, soil hydraulic properties, and soil thermal properties could be jointly estimated using soil temperatures. Instead of using approaches that estimate the model parameters separately, joint model state-parameter estimation approach can significantly reduce the computational cost [*Han et al*., 2014]. They also demonstrated that soil hydraulic properties control the temporal variation of soil moisture, which eventually leads to different soil temperatures. Being able to determine the soil hydraulic and thermal properties in this manner solves the third challenge without the need for time-consuming and labor-intensive field measurements. It was also demonstrated that jointly estimating model state and parameters provide more accurate and robust estimates of the soil moisture. The final challenge, that of uncertainty in the cable depths, was addressed by *Dong et al*. [2016b]. The cable depths were considered as free parameters and jointly updated with other model states and parameters. Tests using both synthetic tests, and point sensors with known depths show that the PBS method can provide accurate cable depth estimates. Most importantly, the soil moisture estimates were only marginally worse than those obtained when the cable depths were perfectly known. By comparing the estimates from four sites with same climatic forcing but different soil textures, they also demonstrated the potential of detecting the spatial variability of the soil moisture and properties using the PBS.

All of the data assimilation developments to date have been tested and developed using synthetic data and observations from point in situ temperature sensors. In this study, the Particle Batch Smoother will be applied to real Distributed Temperature Sensing data from the Soil Moisture Active Passive (SMAP) Marena Oklahoma In-Situ Sensor Testbed (MOISST) [*Cosh et al*., 2010, 2016].

In order to apply the algorithm to real data, techniques that can avoid severe particle weight degeneracy are required to provide accurate estimates. Increasing the number of the particles is usually effective in reducing the effects of particle weight degeneracy if the initially chosen number of particles was too small. But, when 100 or more particles were used, further increasing the number of the particles provides little benefit [*Dong et al*., 2015b]. Using a different likelihood function may also be helpful in avoiding particle weight degeneracy, as shown in the Generic Particle Filter (GPF) approaches [*Sawada et al*., 2015]. However, a factor that determines the shape of the likelihood function (σ in) [*Sawada et al*., 2015] must be determined prior to performing data assimilation, and the appropriate value of this factor is still unknown for DTS applications. Hence, this study will use the tuning factor proposed by *Dong et al*. [2016a] to avoid particle weight degeneracy. The tuning factor tunes the likelihood function and increase the acceptance probability of the particles, can effectively avoid the particle weight degeneracy and provide robust estimates [*Dong et al*., 2016a, 2016b]. Due to the spatial variabilities of soil and vegetation properties and the fact that all the prior guesses were drawn from the same distribution, the error of the forward model may vary in space. Hence, the value of the tuning factor that can provide the optimal estimates may also vary in space. This indicates a reasonable tuning factor has to be determined every meter along the DTS cable.

Due to the limited scale of the prior studies, it was possible to determine a temporally constant tuning factor by trial and error [*Dong et al*., 2016a]. To apply the PBS to real DTS data, an objective, automatic procedure is needed to determine an appropriate tuning factor.

The purpose of this study is twofold. First, an adaptive Particle Batch Smoother (APBS) will be proposed, and tested using a series of synthetic tests. In this APBS algorithm, the tuning factor will be automatically determined to avoid severe weight degeneration. Second, we will evaluate this APBS algorithm using real DTS data. The estimated soil moisture and properties will be validated using data collected at a nearby site.

2. Method and Materials

2.1. Study Area and Data Collection

All data used in this study were collected at the Soil Moisture Active Passive (SMAP) Marena Oklahoma In-Situ Sensor Testbed (MOISST). This is a field site located at the Oklahoma State University Range Research Station approximately 13 km southwest of Stillwater, Oklahoma. The goal of the testbed is to facilitate the validation of remote sensing measurements from SMAP with in situ sensors distributed around the globe [*Cosh et al*., 2010, 2016]. Figure 1 shows the layout of the site. The predominant soil series is Grainola silty clay loam (fine, mixed, active, thermic Udertic Haplustalfs), which are moderately deep, well-drained soils formed in material weathered from shale. However, the soil texture varies significantly with depth and landscape position. Vegetation across much of the site is typical of tallgrass prairie with some localized areas representative of cross timbers vegetation [*Fuhlendorf and Engle*, 2004]. Five-minute meteorological data including precipitation, solar radiation, humidity, air temperature, and wind speed were obtained from the Oklahoma Mesonet site at Marena from April to June 2011 [*McPherson et al*., 2007]. Hourly soil moisture observations from the Hydra probes (Hydra Probe II, Stevens Water Inc., Portland, OR, USA) at depths of 2.5, 5, 10, 20, and 50 cm at Site B (one of four MOISST base sites) were used here. Soil thermal conductivity at saturated soil water content (λ_{sat}) and soil water content at 33 KPa (θ_{33}) were also measured for evaluating the estimated soil thermal and hydraulic properties.

The DTS equipment, solar panels, and two calibration baths were located at Site B. Fiber-optic cables (50/125 μm multimode) were installed at approximately 5, 10, and 15 cm depths along an approximately "hour glass"-shaped path (658m in total). *Dong et al*. [2015a] showed that soil temperatures at two depths provide sufficient information to estimate soil moisture and soil properties. So, here soil temperature observed by the upper two cables will be used.

Cable temperatures were measured using an Oryx DTS (Sensornet, UK), with an integration time of five minutes, and calibrated using the approach outlined by *van de Giesen et al*. [2012]. The relatively high bulk density and clay content of the subsoil, the terracing on the western side of the loop, some rocks near the surface on the eastern side, and the thick vegetation cover made cable installation difficult. Several sections of the cable had to be hand-dug after the plow pass (crossing terrace berms and/or at tight turns). In these sections, the cables depths are too irregular to be used. This study is limited to the DTS data collected along a 71 m transect extending eastward from site B (See Figure 1). This is one of the smoothest sections because

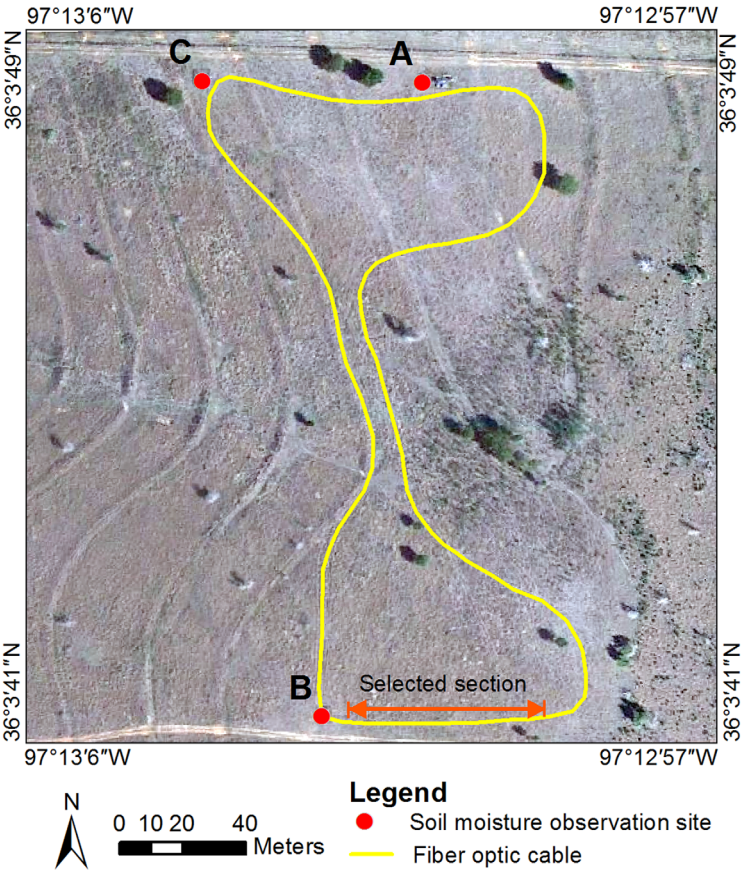

Figure 1. Field layout of DTS cable at Oklahoma MOISST site. Soil moisture and temperature point sensors are installed at Sites A, B, and C. The DTS equipment was housed at Site B.

the surface was flat and the tractor and plow could follow a straight line. Furthermore, the soil texture along this transect is comparable to that at Site B, which also facilitates validation of the results. The DTS temperature data used here were collected from 19 April to 31 May 2011.

2.2. Model State and Parameter Estimation

2.2.1. Forward Model

The forward model used in this study is that presented by *Dong et al.* [2016b], in which a canopy energy balance scheme is included in the Hydrus-1D model. Soil water movement is solved using the Richards equation, and the vapor transport is considered as a flux term in the Richards equation [*Simunek et al.*, 2009]:

$$\frac{\partial\theta}{\partial t}=\frac{\partial}{\partial z}\left[K_{Th}\frac{\partial h}{\partial z}+K_{Lh}+K_{TT}\frac{\partial T}{\partial z}\right]-S \tag{1}$$

where θ is soil water content (m^3m^{-3}) at time t (s), and z is the vertical coordinate (m). The soil hydraulic conductivity curve and soil water retention curve are presented as:

$$K_{Lh}=K_sS_e^l\left[1-(1-S_e^{\frac{1}{m}})^m\right]^2 \tag{2}$$

$$\theta(h)=\begin{cases}\theta_r+\dfrac{\theta_s-\theta_r}{[1+|\alpha h|^n]^m} & h<0\\ \theta_s & h\geq 0\end{cases} \tag{3}$$

where K_s is the saturated hydraulic conductivity (ms^{-1}), K_{Th} and K_{TT} are the isothemal and thermal total hydraulic conductivities, respectively, and K_{Lh} is the isothermal unsaturated hydraulic conductivity for the liquid water, S_e is the effective saturation, l, m, n, and α are empirical shape parameters and θ_r and θ_s are the residual and saturated soil water contents (m^3m^{-3}). Soil heat transport is simulated using the soil heat conduction equation, which also includes the heat convection terms caused by the liquid water and vapor fluxes:

$$\frac{\partial C_pT}{\partial t}+L_0\frac{\partial\theta_v}{\partial t}=\frac{\partial}{\partial z}\left[\lambda(\theta)\frac{\partial T}{\partial z}\right]-C_w\frac{\partial q_LT}{\partial z}-L_0\frac{\partial q_v}{\partial z}-C_v\frac{\partial q_vT}{\partial z}-C_wST \tag{4}$$

where T is soil temperature (K), C_w, C_v, and C_p are the volumetric heat capacities of water, vapor, and moist soil ($Jm^{-3}K^{-1}$), L_0 is the volumetric latent heat of vaporization of liquid water (Jm^{-3}), q_L and q_v are the

flux densities of liquid water and vapor (ms^{-1}), and $\lambda(\theta)$ is apparent soil thermal conductivity ($Wm^{-1}K^{-1}$). The thermal conductivity is approximated using the model proposed by *Lu et al*. [2007].

The soil surface energy balance was solved by the algorithm outlined in *Oleson et al*. [2010]. Its inclusion means that the model can be used to simulate the soil water, heat, and vapor transport in vegetated areas as well as in bare soil conditions. The required model forcing data are incoming shortwave solar radiation, precipitation, air temperature, relative humidity, and wind speed. At depths greater than 50 cm, soil temperature variations during the day are limited [*Bateni and Liang*, 2012]. Hence, a soil depth of 1 m was assumed to ensure the validity of the zero gradient lower boundary condition for soil heat transfer. The time step of the Hydrus-1D simulations is adapted according to the numerical convergence [*Simunek et al*., 2009], and is approximately 1 min in this study.

As shown in equation (1) and (4), soil water and heat transfer are coupled processes. For example, soil thermal conductivity ($\lambda(\theta)$) is a function of soil moisture. This means vertical soil heat transfer will depend on soil moisture conditions. Further, the soil vapor (q_v) transfer, or the soil evaporation, depends on both soil moisture and soil temperatures, which also acts an important link between soil moisture and soil temperature. As a consequence, any factor that affects soil moisture will be eventually reflected in soil temperature observations. Hence, soil hydraulic properties can also be estimated using soil temperatures [*Dong et al*., 2016a]. The improved soil hydraulic properties will, in turn, benefit the forward model, and provide more robust estimates. In addition to soil moisture, the key model parameters to be estimated in the PBS are the soil hydraulic properties (i.e., residual water content (θ_r), saturated soil water content (θ_s), air entry value (α), shape parameter (n), and saturated conductivity (K_s)), soil thermal property (i.e., saturated soil thermal conductivity, λ_{sat}) and leaf area index (LAI). The vegetation optical and structural properties presented by *Oleson et al*. [2010] were used as the nominal values.

2.2.2. Particle Batch Smoother (PBS)

An ensemble of model states is evolved in parallel using the forward model:

$$\mathbf{x}_t^i = f\left(\mathbf{x}_{t-1}^i, \mathbf{u}_t^i, \mathbf{b}_t^i\right) + \mathbf{w}_t^i \tag{5}$$

where $\mathbf{x}_t^i$ is a vector of the model states (θ and T in this study) of the i^{th} particle at time t, $\mathbf{u}_t^i$ is the perturbed forcing data, $\mathbf{b}_t^i$ is a vector of model parameters, $\mathbf{w}_t^i$ is the model error, and f is the forward model [*Moradkhani et al*., 2012]. The model estimates are related to the observation space by:

$$\hat{\mathbf{y}}_t^i = h(\mathbf{x}_t^i) + \mathbf{v}_t^i \tag{6}$$

where $\hat{\mathbf{y}}_t^i$ is the simulated observation vector, h is an operator relating the prior estimated states ($\mathbf{x}_t^i$) to the measured variable, and $\mathbf{v}_t^i$ is the observation error [*Moradkhani et al*., 2012]. Instead of assuming observation depths are perfectly known, it was updated as a free variable. Hence, the operator h was constantly changed according to the estimated observation locations.

The posterior distribution of interest is the joint distribution of the model states (i.e., soil temperature and moisture profile from 0 to 1 m) and model parameters (e.g., soil thermal and hydraulic properties) over a certain time interval (window length). The posterior distribution is mapped using particles with associated weights:

$$p(\mathbf{x}_{t-L+1:t}, \mathbf{b}_{t-L+1:t} | \mathbf{y}_{1:t}) = \sum_{i=1}^{N} w_t^i \delta\left(\mathbf{x}_{t-L+1:t} - \mathbf{x}_{t-L+1:t}^i, \mathbf{b}_t - \mathbf{b}_t^i\right) \tag{7}$$

where $\{\mathbf{x}_{t-L+1:t}^i, \mathbf{b}_t^i\}$ denotes the i^{th} particle, w_t^i is its weight, and δ is Dirac delta function [*Moradkhani et al*., 2005a], and L is the window length. Soil temperatures within a longer window length usually contain more soil moisture and soil property information. However, increasing the window length will also increase the dimension of the estimates at each updating step, which may lead to degraded estimates [*Dong et al*., 2015b]. As shown in *Dong et al*. [2016b], assimilating soil temperature observations within a batch window of 12 h can provide robust soil moisture and property estimates. Since the experiment setting is similar to *Dong et al*. [2016b], a window length of 12 h is also used here. The parameters were assumed to be constant within each batch window, i.e., $\mathbf{b}_{t-L+1:t}^i = \mathbf{b}_t^i$. When the transition prior is used for the proposal distribution for importance sampling [*Dong et al*., 2015b], the weights can be estimated as:

Table 1. Generation of Perturbed Inputs (Soil and Vegetation Property and Forcing) for Each Particle

Variable	Error Distribution	Mean	Std.	Bound
Sand (%)	Uniform			15, 75
Silt (%)	Uniform			0, 100—Sand
ρ_b(g/cm^3)	Uniform			1.1, 1.7
Air temperature (°C)	Gaussian, additive	0	0.05	
Precipitation (mm)	Gaussian, multiplicative	1	× 0.2	
Radiation (W/m^2)	Gaussian, multiplicative	1	× 0.075	-, 1350
Relative humidity (%)	Gaussian, multiplicative	1	× 0.05	-, 100
Wind speed (Km/h)	Gaussian, multiplicative	1	× 0.2	
Vegetation parameters	Gaussian, multiplicative	1	× 0.2	

$$w_t^{i*} \propto w_{t-L}^{i*} p(\mathbf{y}_{t-L+1:t}|\mathbf{x}_{t-L+1:t}^{i}) \quad (8)$$

$$w_t^i = \frac{w_t^{i*}}{\sum_{i=1}^{N} w_t^{i*}} \quad (9)$$

where $w_t^{i,*}$ and w_t^i are the unnormalized and normalized particle weights, respectively, $p(\mathbf{y}_{t-L+1:t}|\mathbf{x}_{t-L+1:t}^{i})$ is the likelihood function, which is calculated as:

$$p(\mathbf{y}_{t-L+1:t}|\mathbf{x}_{t-L+1:t}^{i}) = \prod_{j=t-L+1}^{t} \frac{1}{(2\pi)^{n_o/2} det(\mathbf{R})^{1/2}} e^{\left[-0.5\beta^2(\mathbf{y}_j-\hat{\mathbf{y}}_j^i)^T\mathbf{R}^{-1}(\mathbf{y}_j-\hat{\mathbf{y}}_j^i)\right]} \quad (10)$$

where R is the error covariance of the observations, n_o is the number of soil temperature observation depths, and β is a tuning factor (≤ 1) to avoid particle weight degeneration [*Dong et al*., 2016a,b].

Perturbing the estimated parameter set is usually required to avoid parameter impoverishment [*Moradkhani et al*., 2005b]:

$$\mathbf{b}_t^i = \mathbf{b}_t^i + \epsilon_b \quad (11)$$

where ϵ_b is normally distributed noise with zero mean, and standard deviation (Std) of s. In this study, s is determined as follows:

$$s = max(0, Q_0 - \mathrm{Std}(\mathbf{b}_t)) \quad (12)$$

where Q_0 is a prescribed threshold [*Su et al*., 2011], which is set to be 20% of the initial parameter standard deviation. A discussion of the choice of Q_0 can be found in *Su et al*. [2011], *Aksoy et al*. [2006], and *Dong et al*. [2016b].

Resampling, which replaces the particles that have negligible weights with the particles that have large weights, is needed in the PBS. The systematic resampling method is used in this study, which was considered to outperform other resamping schemes in most scenarios [*Doucet and Johansen*, 2009]. The particles with large weights are more likely to be resampled, and particles with negligible weights will be eliminated. After resampling, all the particle weights were set to be $1/N$. When the prior estimates have large errors, most of the particles will be eliminated and only a few particles will be kept after resampling [*Dong et al*., 2016a]. This dramatically reduced particle range usually cannot encompass the observations and leads to constantly overconfident estimates. To deal with this problem, a tuning factor (β) is usually needed in the PBS [*Dong et al*., 2016a].

2.2.3. Adaptive Particle Batch Smoother

The adaptive particle batch smoother is essentially the same as the PBS algorithm described above, except that the tuning factor for each batch window is determined by maximizing the reliability of the soil temperature estimates. The probabilistic metric of reliability is calculated using the Quantile - Quantile (Q-Q) plot, which indicates whether the estimated uncertainty (particle range or ensemble spread) is appropriate. For each batch window, the quantile of the predictive distribution is calculated at each time step at each observation depth within the batch window [*Moradkhani et al*., 2012; *Dechant and Moradkhani*, 2014]:

$$z_{t_j,j} = \frac{1}{N}\sum_{i=1}^{N} k_i \quad (13)$$

where N is the number of the particles, $z_{t_j,j}$ is the quantile of the predictive distribution calculated at time t_j depth j, $k_i = 1$ when observed soil temperature is larger than the ith particle simulated soil temperature at time t_j, and $k_i = 0$, otherwise [*Madadgar and Moradkhani*, 2014]. In the perfect case, the distribution of $z_{t_j,j}$ should follow the uniform distribution ($U[0, 1]$). If $z_{t_j,j}$ are clustered at the middle range, it indicates that the uncertainty is overestimated. The uncertainty is underestimated when the $z_{t_j,j}$ are clustered around the tails. In the case where $z_{t_j,j}$ is constantly lower/higher than $U[0, 1]$, it indicates the estimates are biased [*Thyer et al*., 2009]. The differences between the $z_{t_j,j}$ and $U[0, 1]$ are measured by reliability (α_r):

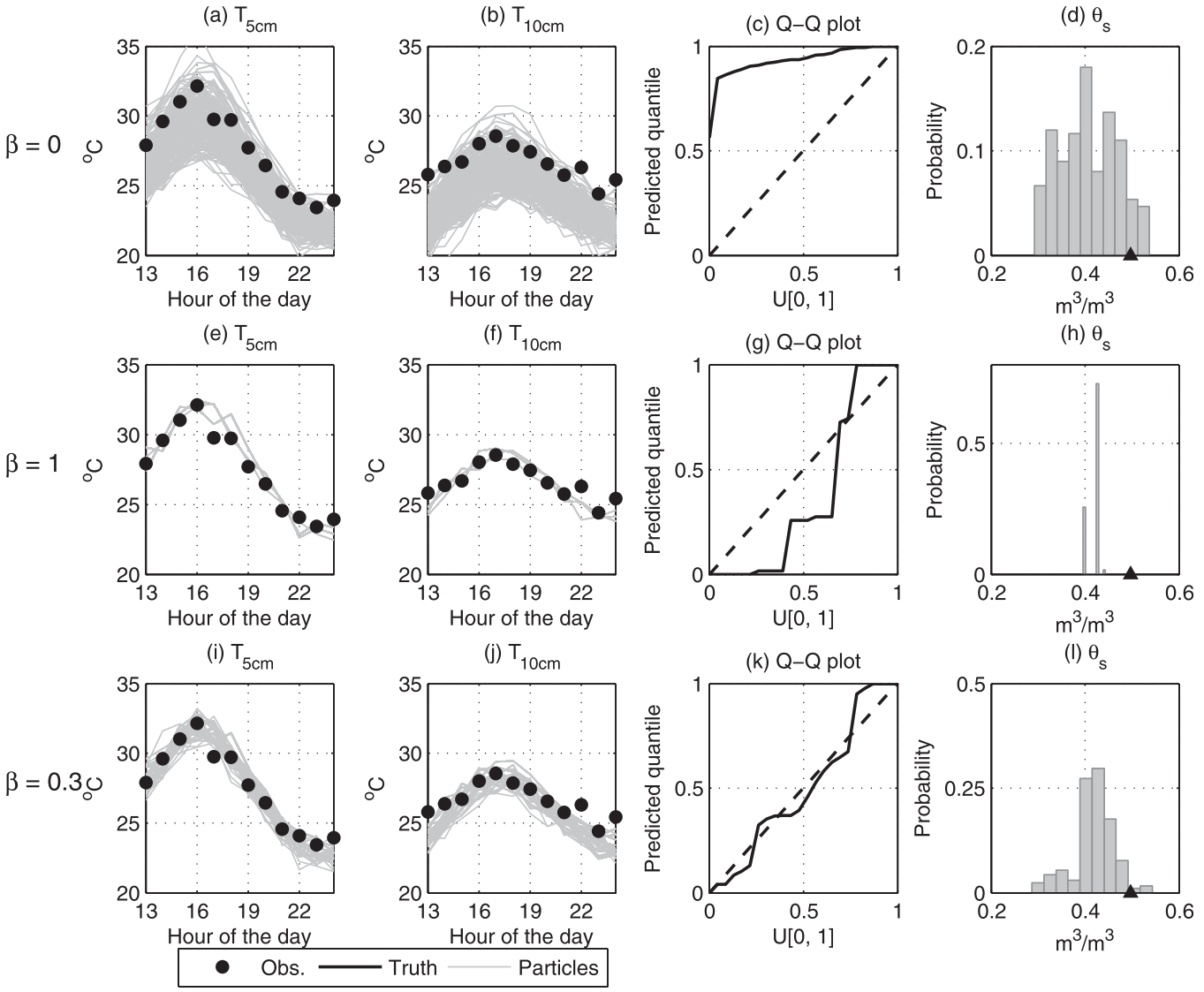

Figure 2. Soil temperature estimates at 5 (first column) and 10 cm (second column), the Q-Q plot (third column), and the posterior distribution of the estimated model parameter using θ_s as an example (fourth column) in one batch window. The top row is the case when $\beta = 0$, which is equivalent to open loop. The second row are the estimates using β=1.0, i.e., no tuning is used. The last row uses an automatically determined β, which is 0.3 in this specific window.

$$\alpha_r = 1 - \frac{2}{n_0 \times n_t} \sum_{j=1}^{n_0} \sum_{t_j=1}^{n_t} |z_{t_j,j} - U[0,1]| \tag{14}$$

where n_t denotes the total number of time steps within the batch window. For example, when hourly soil temperatures were observed at two depths and a window length of 12 h was used, n_0 was two and n_t was 12. Consequently, the reliability of this batch window will be estimated using 24 observations. Reliability (α_r) varies from 0 (zero reliability) to 1 (perfect reliability). *Dong et al.* [2016a] demonstrated that the PBS can provide robust estimates, once this β value is within a reasonable range. Hence, β is varied from 0 to 1 in increments of 0.05 and the optimal β is that which yields the largest reliability in the APBS. In the APBS, rerunning the forward model for the assimilation window is not required. The only increased computational cost compared to the PBS algorithm is the iteration of the weight udpating step and resampling step, which is negligible [*Dong et al.*, 2015b]. Consequently, using APBS is a more cost-effective way of avoiding particle weight degeneracy, compared with simply increasing the number of particles in the PBS. This adaptive approach may be particularly suitable for the cases when particle weight degeneracy is severe, or the prior estimates have large errors. Under such circumstances, the prior distribution may be less capable of

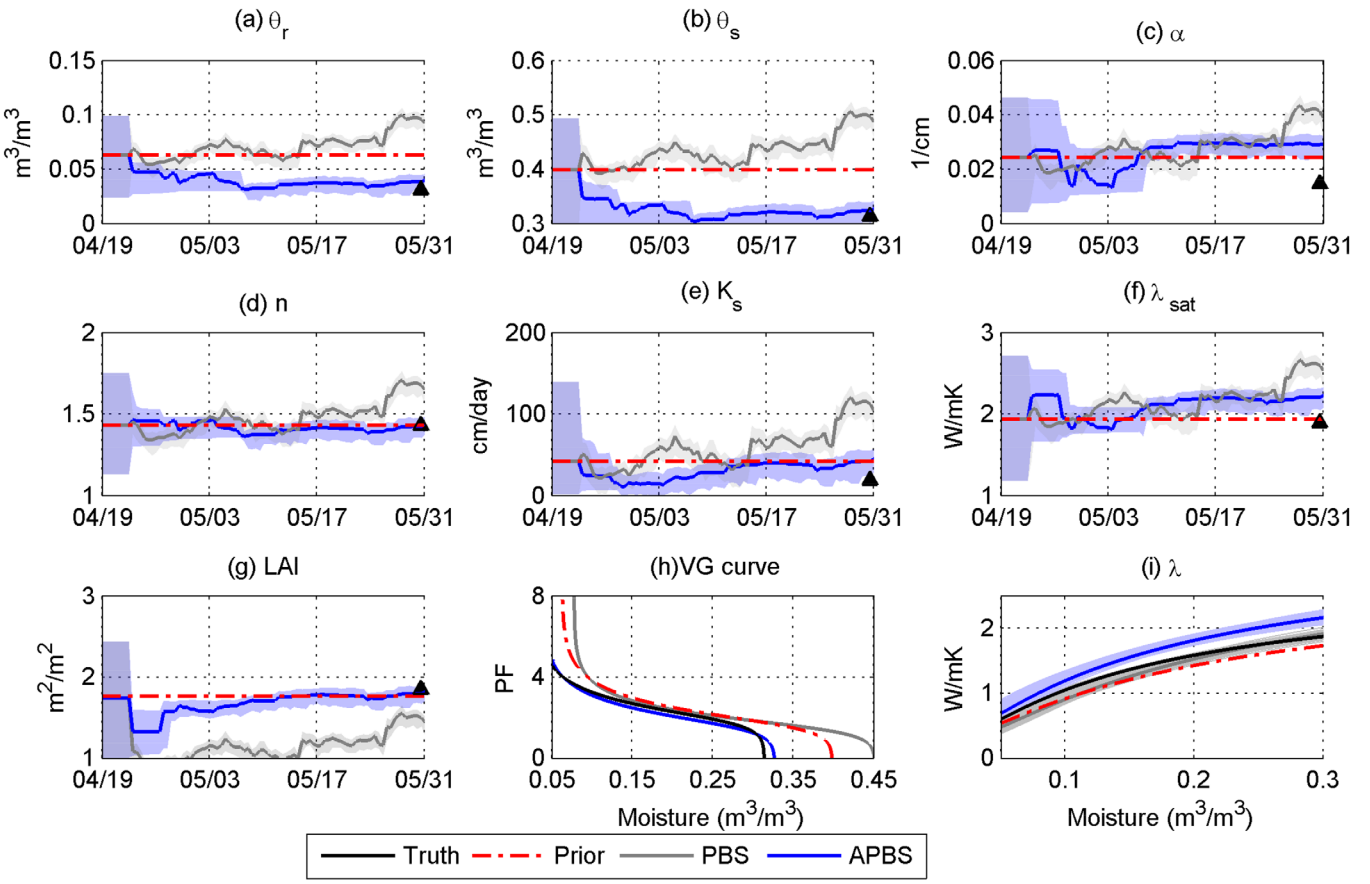

Figure 3. (a–f) The estimated soil hydraulic and thermal properties and (g) LAI. The soil water retention curve and the soil thermal conductivity curve calculated using the estimated soil properties are shown in (h) and (i). The true model parameters are shown at the final time step. The shaded area represents the range of the particles.

encompassing the truth, which also means little model parameter and state information can be inferred from the soil temperatures. Hence, updating the particles using the original PBS (i.e., $\beta = 1$) will unavoidably lead to overconfident estimates and reduced α_r. Further, the parameter estimates will also be overfitted to model or observation errors. While in the APBS method, a small tuning factor will be used to maximize the α_r. Using a small tuning factor will allow the particle range to grow to encompass the observations in the

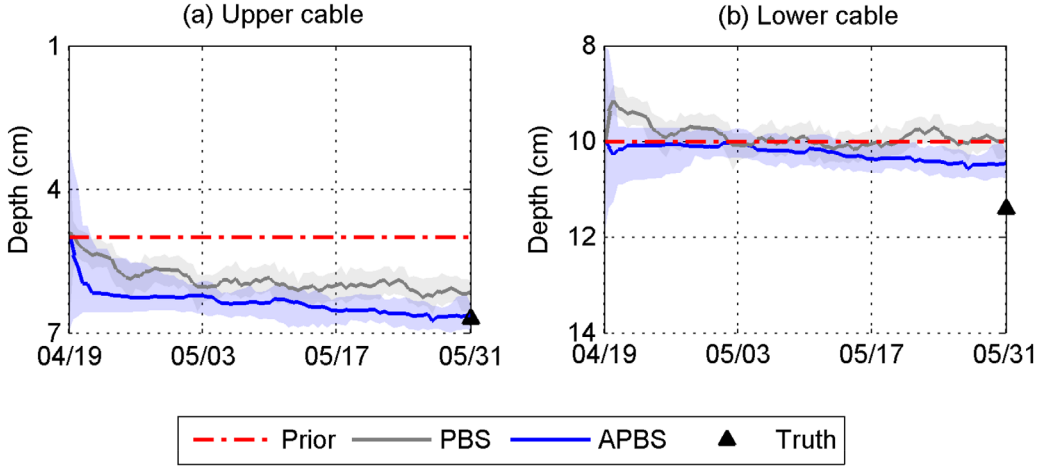

Figure 4. Estimated (a) upper and (b) lower cable depths using the PBS and APBS. The true cable depths are shown at the final time step.

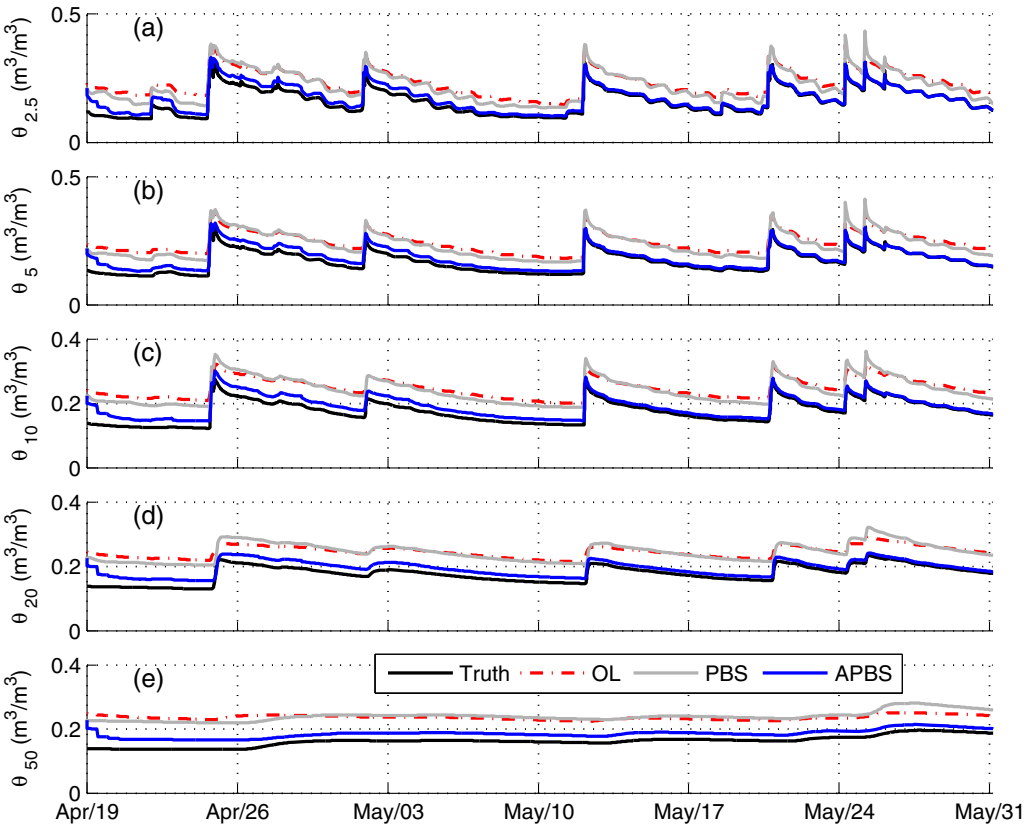

Figure 5. Comparison of the soil moisture estimated using PBS and APBS at 5 depths.

following steps. Further, since a small tuning factor is used, the model parameters are less likely to be overfitted.

2.3. Data Assimilation Experiments

First, we will show the necessity of using the adaptive particle batch smoother (APBS) to avoid severe particle weight degeneracy and to improve the estimates. A single illustrative synthetic test is used to compare the original particle batch smoother (i.e., β=1.0) to the APBS. In this synthetic test, the truth was generated using the forward model with perturbed forcing data (Table 1). Soil textures and soil bulk density drawn

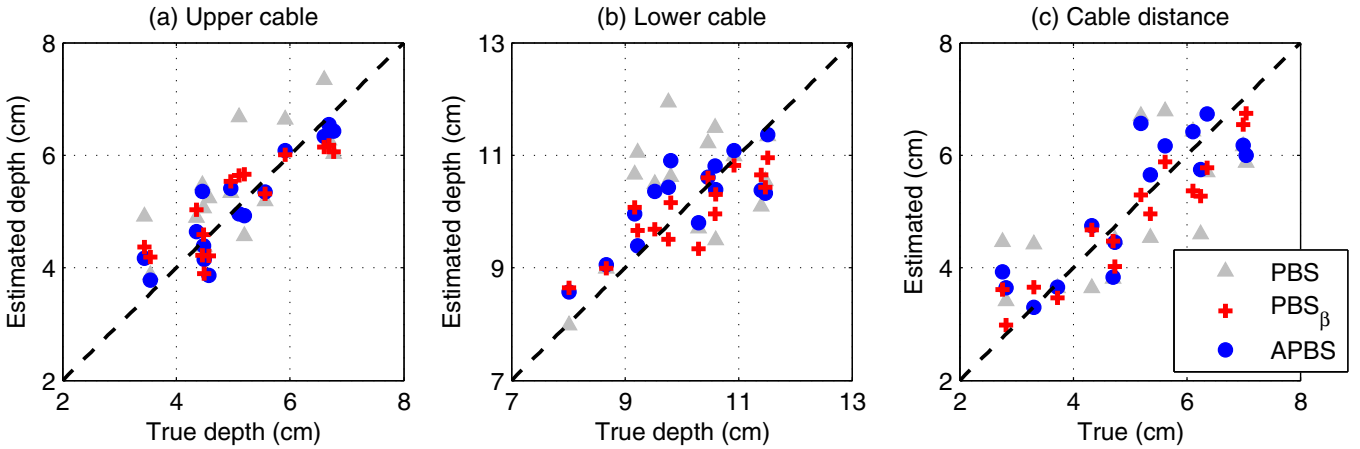

Figure 6. (a and b) Comparison of the true and estimated cable depths, and (c)cable distances using 15 randomly sampled truths.

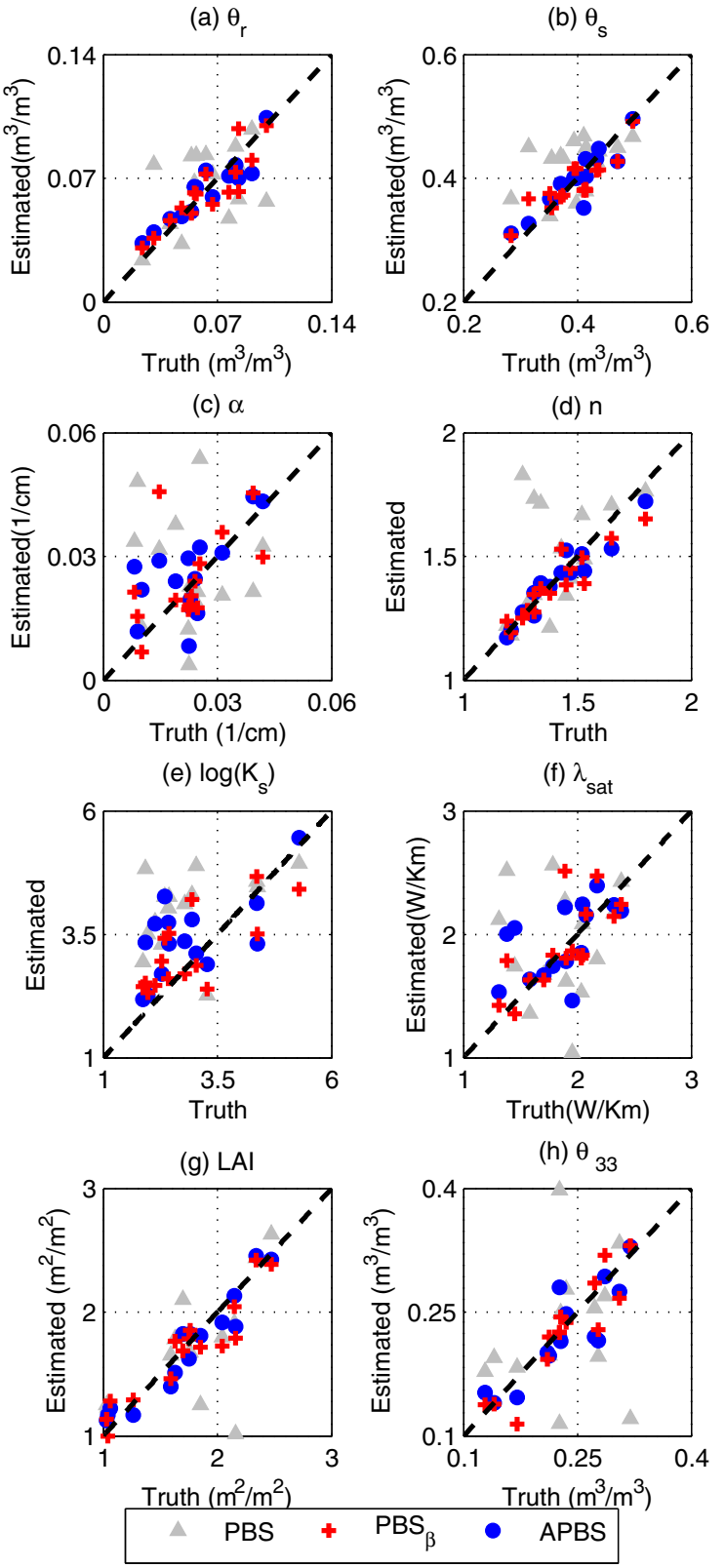

Figure 7. (a–g) Comparison of the true and the estimated model parameters and (h) the θ_{33} calculated using the estimated soil hydraulic properties.

from the distributions described in Table 1 were used to generate the true parameters. To account for uncertainties in the cable depths in real DTS applications, it is assumed the cable depths are poorly known. Hence, cable depth values are drawn from the uniform distributions U[3 cm, 7 cm] and U[8 cm, 12 cm] for the upper and lower cable, respectively. Synthetic DTS observations were generated by adding zero mean Gaussian distributed noise to the synthetic true soil temperatures. As a conservative assumption, the observation error used in this study is 0.5°C. An open-loop run (OL), in which the particles are run in parallel without performing any data assimilation, was used to evaluate the improvement made by the different PBS algorithms. For the OL run, the model parameters were generated using randomly sampled soil properties as described in Table 1. In the PBS algorithms, the initial guess for the cable depths for each particle were drawn from a Gaussian distribution with standard deviation of 1 cm, and mean of 5 cm for the upper cable, and 10 cm for the lower cable. The cable depths were jointly estimated with soil temperature and moisture profiles, soil hydraulic properties (θ_r, θ_s, α, n, K_s), soil thermal property (λ_{sat}), and LAI in both PBS schemes.

Next, we will investigate the robustness of the APBS algorithm using a multiple truth test. We repeated the experiment described above 15 times, where using 15 different truths, generated using randomly sampled model

Table 2. The Correlation of the Estimated and The True Model Parameters Using Different PBS Schemes

Par.	PBS	PBS_β	APBS
θ_r	0.41	0.89	0.91
θ_s	0.44	0.88	0.91
α	−0.15	0.52	0.62
n	0.46	0.93	0.95
K_s	0.54	0.69	0.88
λ_{sat}	0.13	0.74	0.55
θ_{33}	0.37	0.92	0.90
LAI	0.71	0.94	0.96

parameters. *Dong et al.* [2016a] demonstrated that setting β=0.25 in the original PBS algorithm (note as PBS_β) yields significantly improved estimates. A comparison of the PBS_β and the APBS may provide insight to the benefits of using an adaptive tuning factor in the PBS, rather than simply assuming some arbitrary value. Hence, in this multiple truth test, three PBS schemes, i.e., PBS, PBS_β, and APBS, were compared.

Finally, the APBS algorithm was tested using the real DTS data from the SMAP MOISST. The APBS estimated soil moisture and soil properties were evaluated using the data collected from an observation site approximately 70 m away. First, we examined the variability in the estimated cable depths. Then, we validated the estimated thermal conductivity and field capacity against observed values, and compared estimated soil moisture along the cable to that observed with in situ Hydra probes at the nearest enclosure (Site B). Finally, we used the estimated soil moisture to quantify spatial variability in moisture along the cable and consider possible sources of this variability.

Increasing the total number of the particles can increase the diversity of the particles, and hence potentially increase the number of the effective particles (N_{eff}). However, when observations are located at the tails of the priors, most of the particles will be discarded. For these cases, increasing the number of the particles results in little benefits. As shown by *Dong et al.* [2016a,b], 300 particles are sufficient to capture the model state-parameter space after proper tuning. Due to the computational demand, further increasing the number of the particles was not considered. Hence, as a conservative choice for the APBS algorithm, 300 particles were used in this study.

3. Results and Discussion

3.1. An Illustrative Case

Figure 2 illustrates how the value of β influences the Q-Q plot, and hence how the Q-Q plot can be used to determine β adaptively. In the top plot, β=0.0, which means that the state and parameters were not updated. This is equivalent to an open loop simulation. Figures 2a and 2b show that the posterior estimate is biased. As a result, Figure 2c shows that the predicted quantile is constantly above the cumulative uniform distribution. At the other extreme, Figures 2e–2h show what happens when β=1.0. Because the observation error was so small with respect to the a priori estimate, only a few particles were preserved after resampling (Figures 2e and 2f). Consequently, the Q-Q plot shows that the predicted quantiles are clustered in the middle range, which indicates that the estimated posterior is overconfident (Figure 2g). This also indicates that the particle weights are significantly degenerated. As a result, the posterior of the model parameter, e.g., θ_s, is concentrated on a few particles, and therefore cannot encompass the true value (Figure 2h). Figures 2i and 2j show the impact of selecting a tuning factor that maximizes the reliability of the soil temperature estimates. More particles are accepted in the posterior distribution which also benefits the model parameter estimation. Though the mode of the posterior is biased, the range of the posterior is still wide enough to encompass the truth (Figure 2l). In this case, the Q-Q plot shows that predicted quantiles are almost perfectly aligned with those from a uniform distribution (Figure 2k).

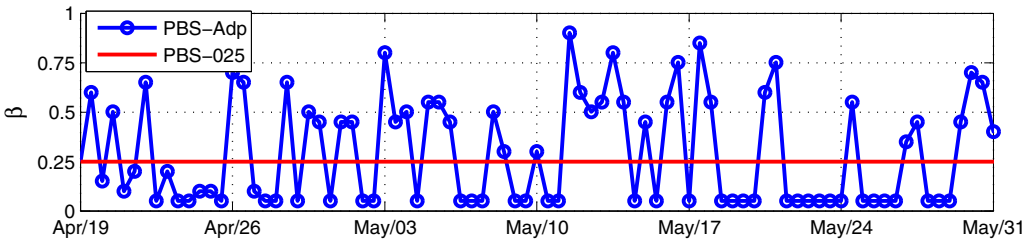

Figure 8. The evolution of the tuning factor (β) in the APBS and the PBS-025 using one single truth for illustration.

Table 3. The RMSE of the Estimated Soil Moisture and Soil Temperature Using Different PBS Schemes at Five Depths[a]

State	App.	2.5 cm	5 cm	10 cm	20 cm	50 cm
Moisture	PBS	0.041	0.042	0.041	0.040	0.042
	PBS_β	0.022	0.023	0.024	0.028	0.032
	APBS	0.022	0.023	0.023	0.026	0.031
Temperature	PBS	0.656	0.541	0.509	0.505	0.494
	PBS_β	0.417	0.342	0.285	0.255	0.251
	APBS	0.339	0.275	0.258	0.253	0.249

[a]The values are averaged from 15 tests using randomly sampled truths.

Figure 3 compares the convergence of the model parameter estimates when β is set to 1.0 (PBS) to the case when β is estimated using the APBS. In this specific illustrative case, the PBS fails to converge to the true parameters (Figures 3a–3g). The evolution of the parameter estimates is also quite unstable, even at the end of the experiment, which suggests that the PBS overfits the model parameter to the model error. The APBS provides significantly improved soil hydraulic properties, compared to the PBS approach (Figures 3a–3e). This yields a nearly perfectly estimated soil water retention curve (Figure 3h). Among the five soil hydraulic properties, the α and K_s parameters provide the poorest agreement with the true values. This is because these two parameters are less sensitive to the soil temperature evolution than the other parameters [*Dong et al*., 2016a]. The prior guessed thermal conductivity, λ_{sat}, is very close to the truth in this specific case. Both PBS and APBS provide degraded estimates of λ_{sat} and that thermal conductivity curve (Figures 3f and 3i). Because the soil moisture drives dynamics in soil thermal properties, the soil hydraulic properties are easier to estimate than the soil thermal properties [*Dong et al*., 2016a]. The prior guessed LAI is already very close to the truth (Figure 3g). Both the PBS and the APBS have converged to the true LAI at the final time step. However, it is noticeable that the estimate from the PBS varies considerably during the simulation period.

The estimated upper and lower cable depths using PBS and APBS for this synthetic, illustrative case are shown in Figure 4. The prior guess for the cable depth of the upper cable was biased by approximately 1.5 cm. Both the PBS and the APBS draw the prior estimate closer to the truth, and result in an error of less than 0.5 cm for both methods. The estimated lower cable depth is less accurate compared to the upper cable in this specific case (Figure 4b). The solar signal is damped exponentially with depth, and hence it is more difficult to estimate the depth of the lower cable [*Dong et al*., 2016b].

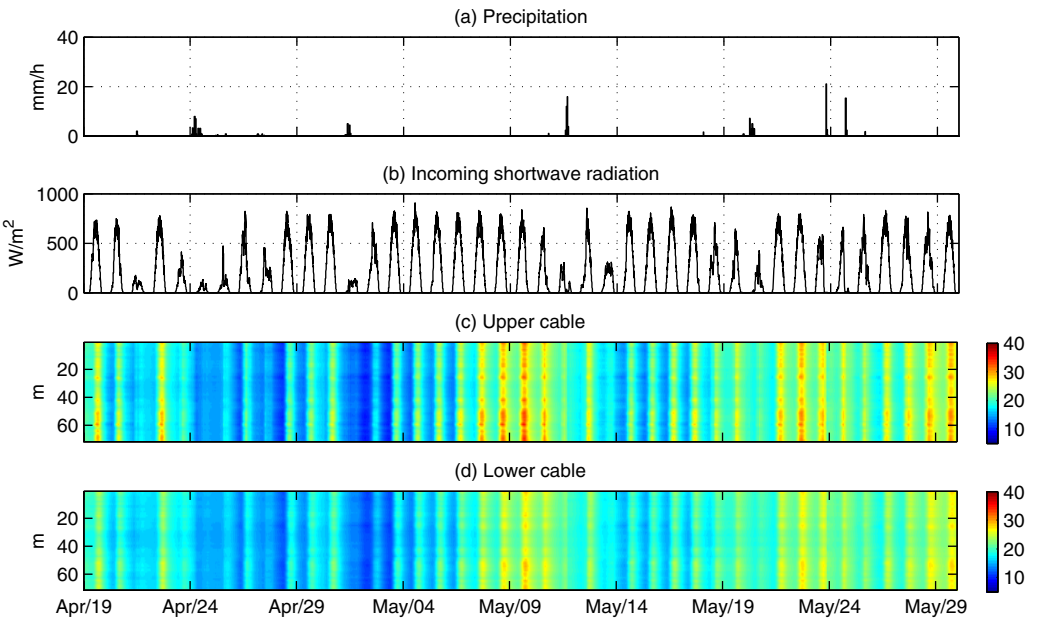

Figure 9. (a) Observed precipitation, (b) solar radiation, and (c and d) soil temperature using two fiber optic cables along a 71 m transect from 19 April and 29 May. The color represents the soil temperature (°C).

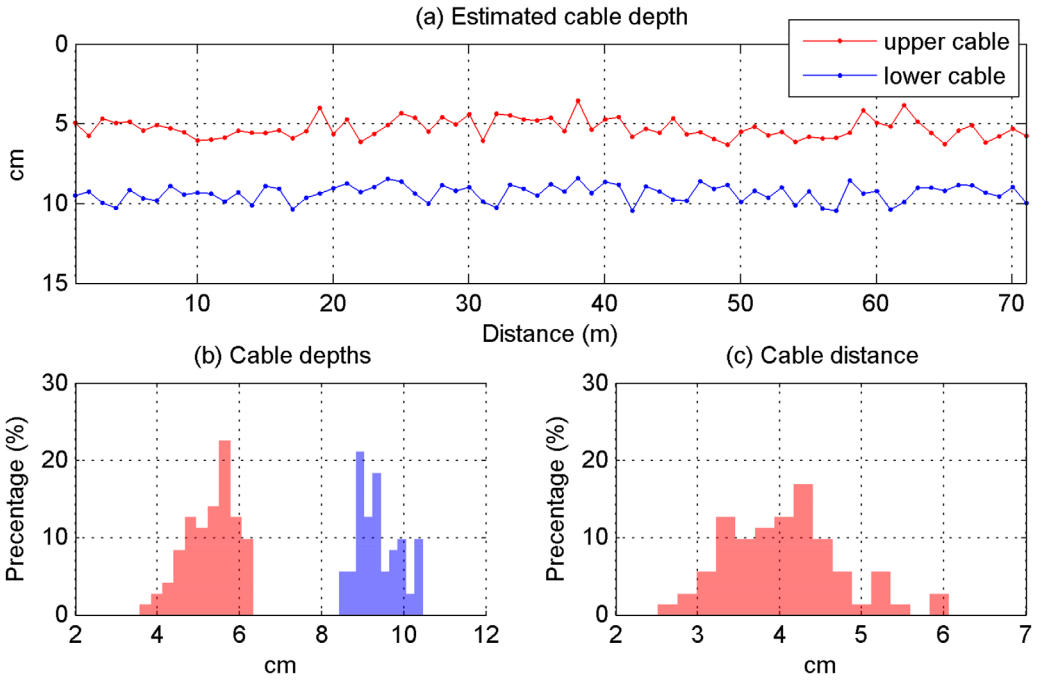

Figure 10. (a) The estimated upper and lower cable depths along a 71 m DTS transect, (b) the distribution of the estimated 71 m cable depths, and (c) the distribution of the estimated cable distances.

Figure 5 shows the soil moisture estimates using the two PBS schemes. Because the PBS yielded little improvement in the soil hydraulic properties compared with the prior (Figure 3), the estimated soil moisture from the PBS is very similar to the OL estimates at all depths. On the other hand, the APBS benefits from the near perfect soil property estimates from approximately 10 May onward (Figure 3). Hence, it provides very accurate surface soil moisture estimates. Soil moisture at depth has little response to the climatic forcing at the upper boundary during the simulation period. Furthermore, only 5 and 10 cm soil temperatures were assimilated in this study, which has limited correlation with the soil moisture in the deeper profiles. Thus, the APBS algorithm mainly benefits the root zone soil moisture estimates through model physics, i.e., increasing or decreasing soil water content at surface will eventually lead to a wetter or drier root zone soil moisture. Hence, the impact of the errors in the initial condition increases with depth (e.g., Figure 5e). This may indicate longer-term simulations are necessary for the PBS algorithms to yield to improvements at depth. The estimated soil moisture at depth might be improved by employing bias correction methods analogous to those employed by *Ryu et al.* [2009], *De Lannoy et al.* [2007], *Dee and Da Silva* [1998], and *Monsivais-Huertero et al.* [2016].

3.2. A Multiple Truth Comparison of Different PBS Schemes

The previous section showed results from a single synthetic case. Figures 6 and 7, and Table 2 summarize the results when this experiment was repeated 15 times for different synthetic "truths." Figure 6 shows a comparison of the true and the estimated cable depths when β is set to 1.0 (PBS), a fixed value of 0.25 (PBS_β) or determined using the adaptive PBS (APBS). The PBS_β and APBS estimated cable depths and separation distances with similar accuracies, which were better than that of PBS approach. Similar to the illustrative case, the depth of the lower cable proved difficult to estimate.

The estimated model parameters and the correlations between the estimates and the truths are shown in Figure 7 and Table 2. In general, the PBS estimated model parameters are the least correlated with the true parameters, compared with the PBS_β and APBS. This is consistent with a previous study [*Dong et al.*, 2016a], which demonstrated that when no tuning factor is used (i.e., PBS), the PBS algorithm will have severe weight degeneration problems, which eventually lead to unreliable estimates. The PBS_β and APBS provide similar results. In general, the correlations between the truth and the APBS estimated model parameters are higher than that of PBS_β.

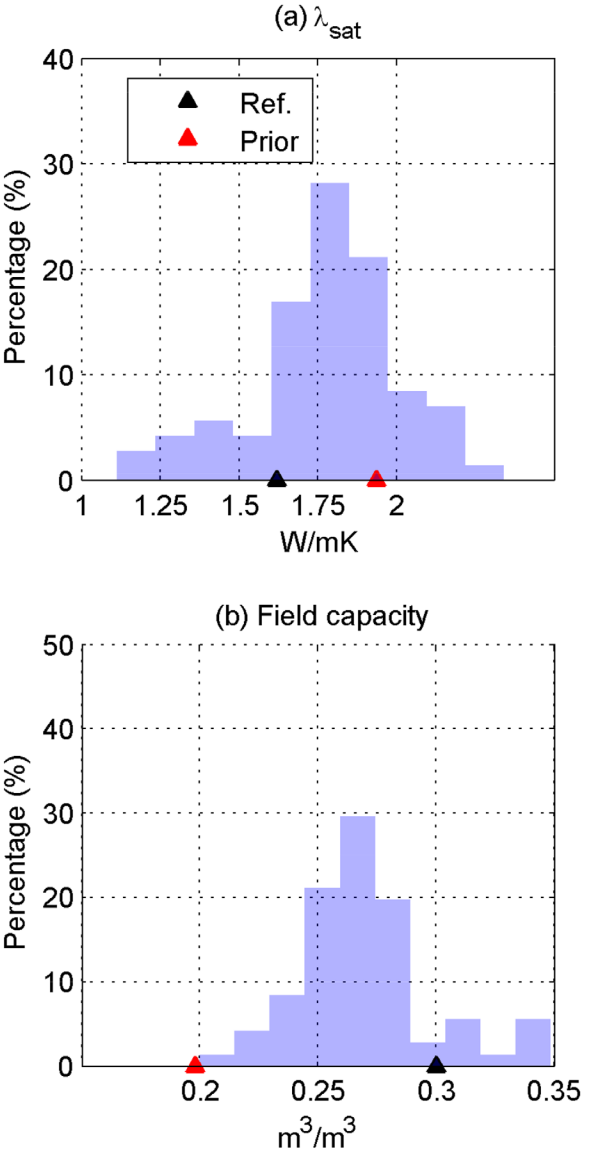

Figure 11. (a) The distribution of the estimated soil thermal property (λ_{sat}) and (b) soil hydraulic property (θ_{33}) along the 71m DTS transect.

The evolution of β values from a single truth in the APBS is presented to provide a more detailed comparison of the APBS and PBS$_\beta$ method (Figure 8). As shown in section 2.2.3, the use of β is essential to ensure the particle range is just wide enough to encompass the observations. If the observation is already within the prior range, a β value as high as 0.9 will encompass the observation. On the contrary, when the particle ranges are too narrow to encompass the observations (i.e., particle degeneracy), zero or small β value should be used to breed the particles. Hence, the optimal value of β is not a simple function of the state, forcing, or parameter, but a combination of circumstances that may lead to particle degeneration, e.g., the model structural error, the model forcing uncertainties, and the variance and the accuracy of the model parameters. As a consequence, the value of β or the factors that leads to particle weight degeneracy cannot be decoded by simply using the model forcing or soil state observations. Assuming a single value of 0.25 for β reduces the likelihood that the observation is beyond the particle range, but does not ensure this to be the case.

As a result of the similarity in the soil properties, the PBS$_\beta$ and APBS also provide very similar soil moisture estimates (Table 3). Using the PBS yields the poorest soil moisture estimates, the RMSE of which is approximately twice as high as that of the PBS$_\beta$ and APBS. The necessity of using the tuning factor in the PBS is also shown in the soil temperature estimates. The RMSE of PBS estimated soil temperature is above 0.5°C for depths $\leq$ 20cm, which is even larger than the observation error. Using a tuning factor of 0.25 (PBS$_\beta$) can significantly avoid the particle weight degeneration, and leads to a sharp decrease in the soil temperature RMSE. When the adaptive tuning factor is used (APBS), the soil temperature RMSE were further reduced at depth above 10 cm.

The results from the multiple truth tests presented in this section show several key points in successfully implementing the PBS algorithm. The PBS algorithm updates the model states and parameters by placing more weight on the particles that have a better fit to the observations, and discarding the particles that have little weight. Hence, when the range of the particle estimates is small, the prior distribution mapped by the PBS is very unlikely to contain the global optimal parameter sets. As a result, the PBS estimates can be unreliable, which is consistent with a previous study [*Dong et al.*, 2016a]. The PBS$_\beta$ uses a tuning factor of 0.25, which makes the particles more acceptable in the resampling process. This will allow the prior distribution for the model states and parameters to have heavier tails, which is more likely to encompass the observations. As a result, the estimates were greatly improved compared to those from the PBS (Tables 2 and 3). However, until now, the tuning factors had been obtained by trial and error, and assumed to be constant in time. In order to implement the PBS to real DTS data, it is essential that the tuning factor can be

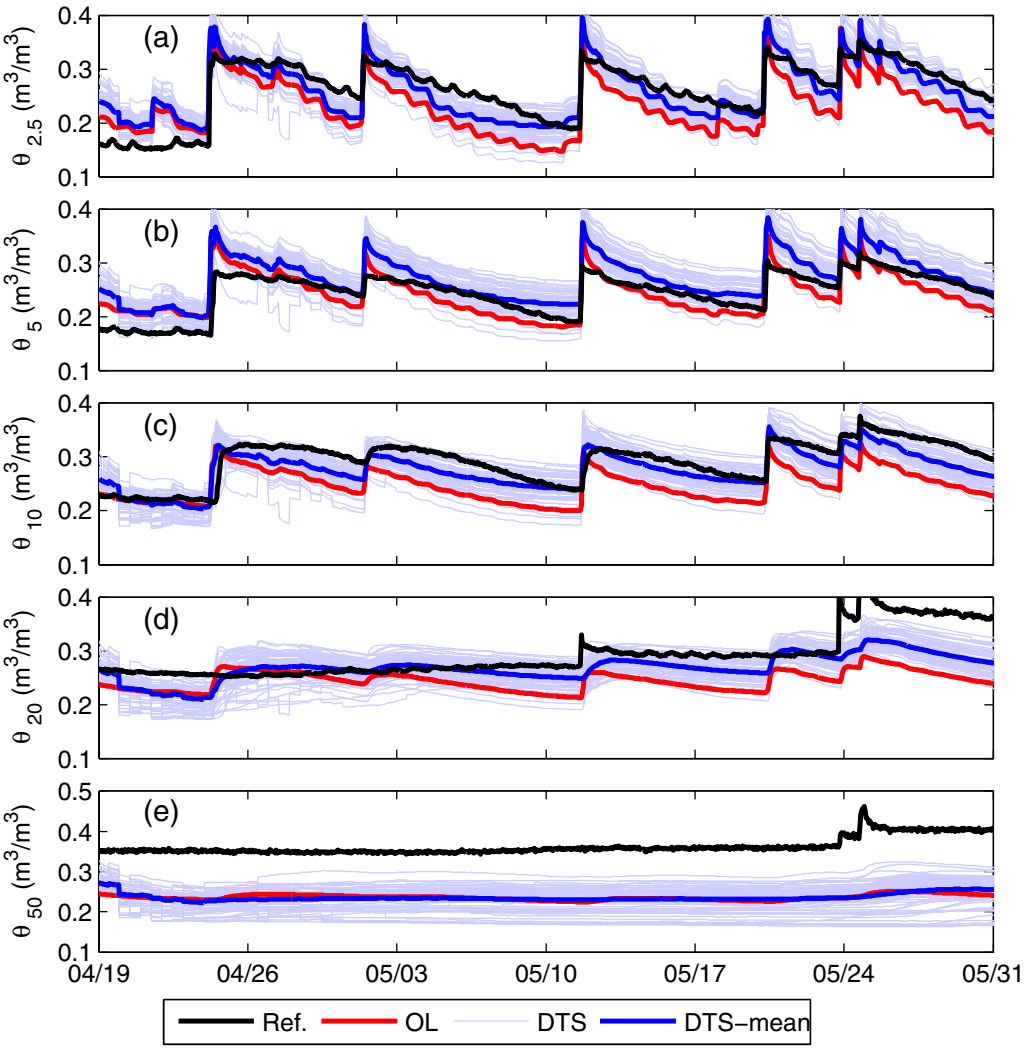

Figure 12. The estimated soil moisture along the 71 m DTS transect at five depths. The black solid line is the soil moisture measured at site B. Each thin blue line represents soil moisture estimates for one meter of cable, and the mean estimated soil moisture of the 71 m cable is shown as the blue solid line.

determined objectively and automatically for each section of cable. The APBS can also be considered as a more statistically meaningful way of tuning the PBS algorithm. For each batch window, the APBS finds a β value that gives the largest reliability of the soil temperature estimates, i.e., a β value that optimally addresses uncertainties of the estimates. For example, when the particle spread is small, small tuning factors should be used to breed the particles. Conversely, when the particle spread is large, a large tuning factor can be used to make full use of the soil temperature information. Thus, the APBS is shown to be superior than PBS_β in most of the model state and parameter estimates.

3.3. Implementing APBS in a Real DTS Experiment

Figure 9 shows the temperatures measured at approximately 5 and 10 cm using DTS from 19 April 2011 to 29 May 2011. The diurnal cycles of the observed soil temperatures due to solar radiation (Figure 9b) are clearly visible. The daily amplitude of soil temperature is lower on days with precipitation and low radiation (e.g., 24–29 April). Some spatial variation is observed, e.g., lower temperatures between 30 and 42 m, and higher temperature between 50 and 60 m. These variations could be due to differences in soil texture and/or vegetation cover, and variations in cable depths.

Figure 10 shows the estimated cable depths along the 71 m DTS transect at the SMAP MOISST site. The average depths of the upper and lower cables are 5.28 and 9.35 cm, respectively. The average estimate of

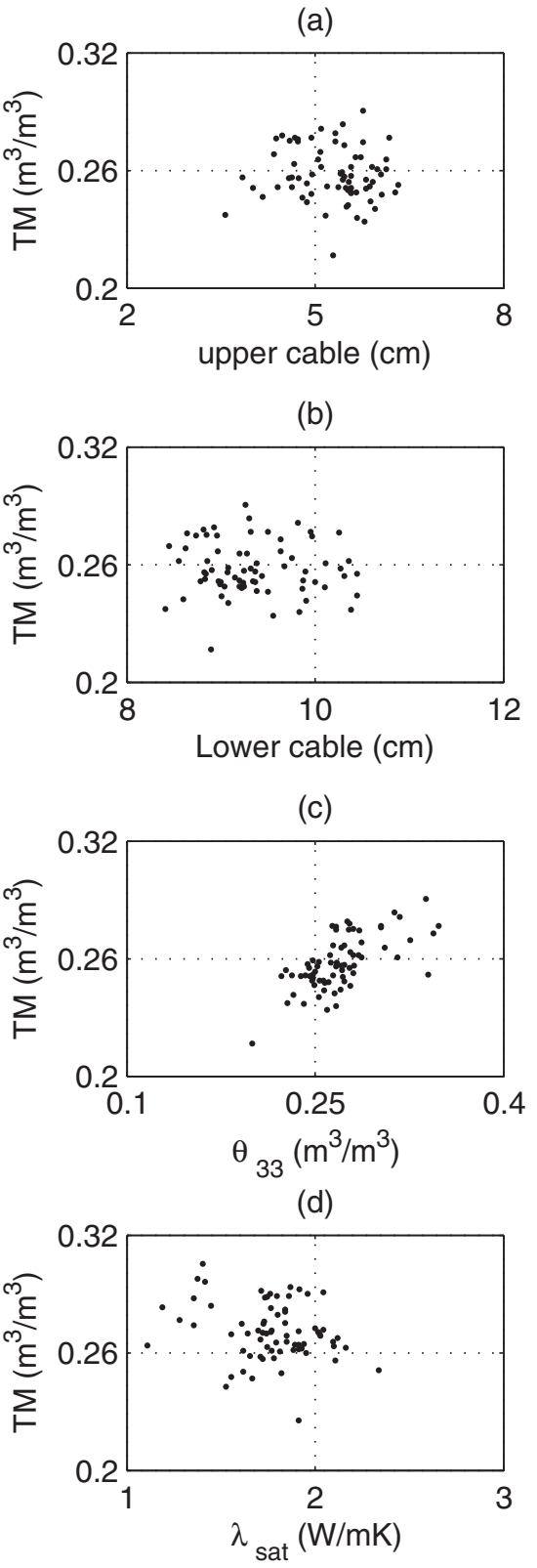

Figure 13. (a and b) The temporal mean (TM) of soil moisture at 2.5 cm as a function of estimated cable depths, (c) soil hydraulic, and (d) thermal properties. Each symbol represents the temporal mean of 2.5 cm soil moisture estimated at one meter of the DTS cable.

the separation distance between the two cables is approximately 4 cm. These estimates are plausible given the plow configuration. The spatial variability can be attributed to the impact of soil roughness on the cable installation.

Histograms of the estimated saturated soil thermal conductivity (λ_{sat}) and θ_{33} along this 71 m DTS transect are shown in Figure 11. These are the only two parameters for which validation measurements were available at the nearby site B. The prior guessed λ_{sat} is approximately 1.9 W/mK, which is significantly higher than the measured value. The average of the APBS estimated λ_{sat} values was drawn closer to the reference value, with an average of 1.77 W/mK along this 71 m transect.

The mean of the prior estimated θ_{33} is approximately 0.2 m^3/m^3, which is significantly lower than the field measured reference value. When soil temperature observations from the DTS are assimilated, the mean of the estimated θ_{33} of this 71 m transect is 0.27 m^3/m^3.

The time series of the estimated soil moisture using the DTS observed soil temperature is shown in Figure 12, and compared to the observed soil moisture at the reference site. Due to the significantly biased estimated soil hydraulic properties (Figure 11b), the OL is biased compared to the reference site. When soil temperature is assimilated, the APBS removes the biases between the OL and the reference soil moisture at depths above 20 cm. At 50 cm, the soil moisture estimates are dominated by the initial guess for soil moisture. Therefore, no significant improvement is shown in the APBS estimates, compared to the OL.

In Figure 13, the mean soil moisture in each meter of DTS cable is plotted against key soil properties as well as the cable depths in order to rule out any relationship between the estimated soil moisture and the estimated cable depths. From Figures 13a and 13b, it is clear that there is no correlation between the estimated cable depths and the temporal mean of the soil moisture. This means the spatial pattern in soil moisture is not merely an artefact of uncertainty in the cable depth estimation. On the other hand, the temporal mean of the soil moisture along this 71 m transect has the strongest correlation with θ_{33}. This suggests that the spatial variability of the soil moisture across this transect is primarily attributed to the spatial variability of the soil hydraulic properties.

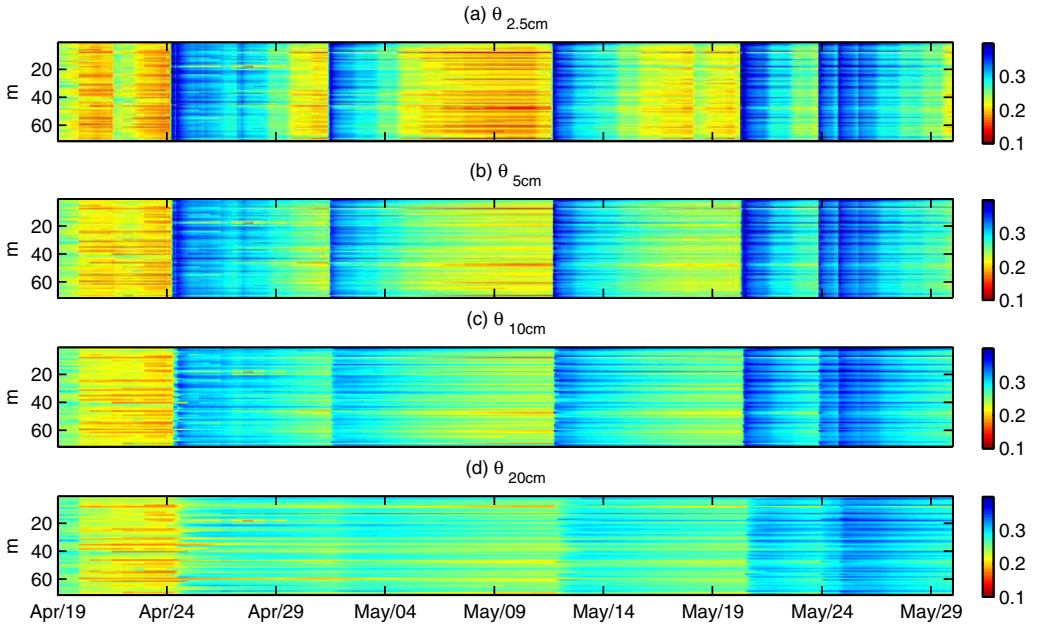

Figure 14. (b–e) Soil moisture estimates along a 71 m DTS transect at four depths. The color denotes the value of soil moisture.

Figure 14 shows the soil moisture at depths $\leq$ 20 cm across this transect. Soil moisture along this 71 m of DTS cable at 2.5 cm shows a fast response to the climatic forcing. The impact of the forcing dramatically decreases with depth. Hence, the rapid increases in wetness following precipitation and the slow drying down are more evident in the soil moisture at 2.5 cm. The horizontal stripes apparent in the soil moisture estimates represent spatial variability. As shown in Figure 13, variance of the estimated soil moisture can be well explained by the soil hydraulic properties, which is likely due to variations in soil texture. Below 20 cm, little spatial or temporal soil moisture variability is observed. Similar to Figure 13, soil moisture estimates at this depth still have a strong correlation with estimated soil hydraulic properties (θ_{33}), with a correlation coefficient of 0.48. This means the variations of soil moisture due to spatial patterns in soil texture are still visible. Other factors, e.g., microtopography and vegetation, may also have impacts on the soil moisture spatial variability.

Figures 15a and 15b show the evolution of the statistics of the soil moisture spatial variability along this transect, taking 2.5 cm soil moisture for illustration. No clear temporal pattern is shown in the standard deviation of soil moisture, except that the spikes after rainfall. In data assimilation, no perturbation for precipitation is used for days with zero precipitation, while a large multiplicative error is used for large precipitation events. Hence, the larger standard deviation of the soil moisture is likely to occur during or shortly after rainfall events. The standard deviation of the soil moisture is not shown to be a strong function of the areal mean soil moisture (Figure 15c). It also seems the soil moisture standard deviation slightly increases with increased mean soil moisture, while several previous studies show soil moisture standard deviation reaches the peak value when areal mean soil moisture is in the range of 0.17–0.23 m^3/m^3 [e.g., *Vereecken et al*., 2007; *Famiglietti et al*., 2008]. However, various relationships between soil moisture and standard deviation at intermediate scales were also found in previous studies, as summarized in *Brocca et al*. [2007]. The time scale used for deriving standard deviation-mean soil moisture relationships also varies widely, which can range from a few days to one year or longer, as summarized in *Famiglietti et al*. [1998]. This might indicate the standard deviation-mean soil moisture relationship is sensitive to observation errors, soil properties, seasonal impacts, and climatic forcing of the study area. The DTS data presented in this study are approximately 40 days. Hence, it might be helpful to further test the validity of the standard deviation-mean areal soil moisture relationship detected along this transect by collecting longer DTS records.

The coefficient of variation (CV) of the soil moisture along this transect has a clear temporal signature (Figure 15b). In general, the CV of soil moisture at 2.5 cm is low during rainfall events (e.g., 1 May). The value of CV increases during the dry down period (e.g., 1–12 May). This makes sense as soil moisture is essentially

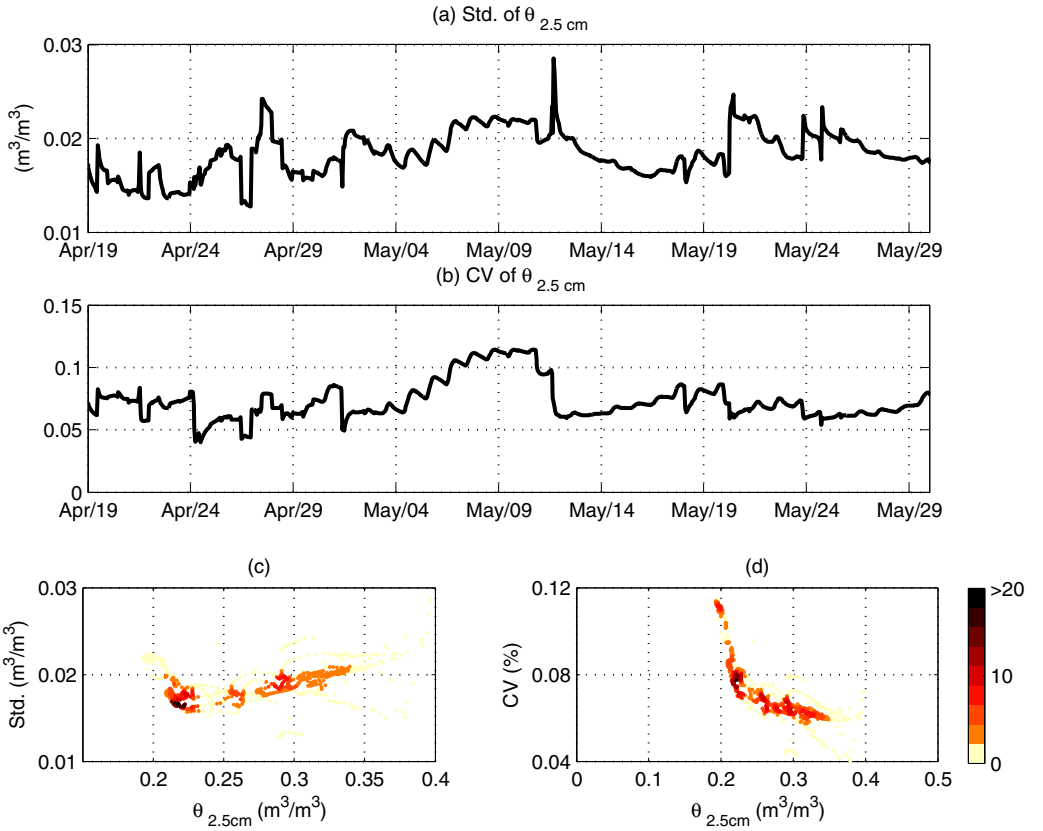

Figure 15. (a) The time series of the standard deviation and (b) coefficient of variation of 2.5 cm soil moisture. (c) The standard deviation and (d) coefficient of variation as a function of areal mean soil moisture.

reinitialized by precipitation events, with sharply increased soil water content and decreased CV. The CV of the soil moisture will start to increase again in the subsequent dry down process. CV is also shown to be a strong function of the areal mean soil moisture (Figure 15d), which is consistent with previous studies [e.g., *Famiglietti et al.*, 2008; *Brocca et al.*, 2010; *Bell et al.*, 1980]. This highlights the potential of using DTS to observe and monitor the temporal and spatial soil moisture variability.

4. Conclusion

In this study, we demonstrated the potential of mapping meter resolution soil moisture and soil properties along a 71 m DTS fiber optic cable using an adaptive Particle Batch Smoother (APBS). The estimated soil moisture and properties were evaluated using field measurements at a nearby site. Results show that the coefficient of variation and areal mean soil moisture relationship are consistent with previous studies [e.g., *Famiglietti et al.*, 2008; *Brocca et al.*, 2010; *Bell et al.*, 1980]. This indicates that the high-resolution (spatial: 1 m, and temporal: 1 h) soil moisture pattern mapped using the DTS has the potential of providing insight into the spatial and temporal evolution of soil moisture. This is the first study that tests the data assimilation algorithms using real DTS data collected from a complex field installation, and demonstrates the feasibility of assimilating DTS observations for high-resolution soil moisture monitoring. The high-resolution soil moisture information derived from DTS could improve our understanding of soil moisture scaling techniques, e.g., in *Crow et al.* [2012], and in particular will facilitate the validation of the downscaled soil moisture products [e.g., *Kim and Barros*, 2002; *Piles et al.*, 2011; *Peng et al.*, 2015]. In addition to soil moisture, high-resolution soil properties and vegetation properties (LAI) can also be obtained, which are of potential interest for modeling and experimental studies [e.g., *Hazenberg et al.*, 2015; *Niu et al.*, 2014; *Wood et al.*, 2011].

The presented algorithm assumes the soil hydraulic and thermal properties are uniformly distributed in the profile (from 0 to 1 m). As tested using data collected from four heterogeneous soil texture profiles in *Dong*

et al. [2016b], limited impacts were shown on the estimates at the shallow depths, when the assumption of homogeneous soil texture profile is violated. However, there is a need to further explore the impacts and the potential solutions of estimating soil moisture using soil temperatures at places where the soil hydraulic property profiles are strongly heterogeneous in the top 10 cm. The topography of the study area is flat, and the ground water table is relatively deep. Hence, minimal lateral water flow is expected, particularly at shallow depths. However, at locations where lateral soil moisture transport is significant, an alternative forward model (e.g., Hydrus-2D) should be used to account for lateral moisture transport and the sate vector should include sates and soil properties along the cable.

Due to the difficulties in installing the cable at this site with relatively uneven terrain and dense vegetation, the present study used data collected by only part of the DTS cables. The maturity of fiber optic cable installation techniques in recent years [*Sayde et al*., 2014] may be helpful in providing high-quality DTS observed soil temperature for cables up to kilometers in length. Using hourly measured DTS soil temperature data at two shallow depths already yields quite promising results. This suggests that hourly DTS data is sufficient, which will significantly reduce the data management and processing efforts in the large scale DTS experiments.

In this study, an adaptive PBS approach (APBS) was presented that automatically tunes the PBS to avoid severe weight degeneracy and improve parameter estimation. This obviates the need to assume that the tuning factor is a constant, and allows the tuning factor to be determined "on-the-fly" in a statistically meaningful way. The proposed APBS approach should also be valuable in other smoother applications in which parameter estimation might be desirable e.g., stream flow prediction, snow water equivalent estimation, and soil moisture reanalysis [e.g., *Moradkhani et al*., 2005a; *Dechant and Moradkhani*, 2011; *DeChant and Moradkhani*, 2012; *Margulis et al*., 2015; *Dunne and Entekhabi*, 2005; *Montzka et al*., 2011; *Yan et al*., 2015].

Acknowledgments

The soil moisture and soil property data used in the present study may be accessed by contacting T.E. Ochsner and M.H. Cosh. The first author was financially supported for his Ph.D. research by the China Scholarship Council with the project reference number of 201206040043. The contribution of T.E. Ochsner was funded by the Oklahoma Agricultural Experiment Station. The SMAP MOISST site was made possible by contributions from the USDA-ARS Hydrology and Remote Sensing Laboratory, Beltsville, MD, and from NASA. The creation of the MOISST site was initiated by M.H. Cosh, and the site is maintained by C. Stansberry and the Oklahoma State University Range Research Station. We also thank the Center for Transformative Environmental Monitoring Programs (CTEMPs. org, NSF grant 1129003) for their support, Jop Janssen and Lucas Williamson for their work for installing the cables, and Jingnuo Dong at Oklahoma State University for her support in DTS data collection.

References

Aksoy, A., F. Zhang, and J. W. Nielsen-Gammon (2006), Ensemble-based simultaneous state and parameter estimation in a two-dimensional sea-breeze model, *Mon. Weather Rev.*, *134*(10), 2951–2970, doi:10.1175/MWR3224.1.

Bateni, S., and S. Liang (2012), Estimating surface energy fluxes using a dual-source data assimilation approach adjoined to the heat diffusion equation, *J. Geophys. Res.*, *117*, D17118, doi:10.1029/2012JD017618.

Bell, K. R., B. Blanchard, T. Schmugge, and M. Witczak (1980), Analysis of surface moisture variations within large-field sites, *Water Resour. Res.*, *16*(4), 796–810, doi:10.1029/WR016i004p00796.

Brocca, L., R. Morbidelli, F. Melone, and T. Moramarco (2007), Soil moisture spatial variability in experimental areas of central Italy, *J. Hydrol.*, *333*(2), 356–373, doi:10.1016/j.jhydrol.2006.09.004.

Brocca, L., F. Melone, T. Moramarco, and R. Morbidelli (2010), Spatial-temporal variability of soil moisture and its estimation across scales, *Water Resour. Res.*, *46*, W02516, doi:10.1029/2009WR008016.

Chen, Y., K. Yang, J. He, J. Qin, J. Shi, J. Du, and Q. He (2011), Improving land surface temperature modeling for dry land of china, *J. Geophys. Res.*, *116*, D20104, doi:10.1029/2011JD015921.

Ciocca, F., I. Lunati, N. Van de Giesen, and M. B. Parlange (2012), Heated optical fiber for distributed soil-moisture measurements: A lysimeter experiment, *Vadose Zone J.*, *11*(4), doi:10.2136/vzj2011.0199.

Cosh, M. H., T. Ochsner, J. Basara, and T. J. Jackson (2010), The SMAP in situ soil moisture sensor testbed: Comparing in situ sensors for satellite validation, in *2010 IEEE International Geoscience and Remote Sensing Symposium (IGARSS)*, pp. 699–701, IEEE, Honolulu, Hawaii, doi:10.1109/IGARSS.2010.5652389.

Cosh, M. H., et al. (2016), The soil moisture active passive Marena, Oklahoma, in situ sensor testbed (smap-moisst): Testbed design and evaluation of in situ sensors, *Vadose Zone J.*, *15*(4), doi:10.2136/vzj2015.09.0122.

Crow, W., and D. Ryu (2009), A new data assimilation approach for improving runoff prediction using remotely-sensed soil moisture retrievals, *Hydrol. Earth Syst. Sci.*, *13*(1), 1–16, doi:10.5194/hess-13-1-2009.

Crow, W. T., A. A. Berg, M. H. Cosh, A. Loew, B. P. Mohanty, R. Panciera, P. de Rosnay, D. Ryu, and J. P. Walker (2012), Upscaling sparse ground-based soil moisture observations for the validation of coarse-resolution satellite soil moisture products, *Rev. Geophys.*, *50*, RG2002, doi:10.1029/2011RG000372.

De Lannoy, G. J., R. H. Reichle, P. R. Houser, V. Pauwels, and N. E. Verhoest (2007), Correcting for forecast bias in soil moisture assimilation with the ensemble Kalman filter, *Water Resour. Res.*, *43*, W09410, doi:10.1029/2006WR005449.

Dechant, C., and H. Moradkhani (2011), Radiance data assimilation for operational snow and streamflow forecasting, *Adv. Water Resour.*, *34*(3), 351–364, doi:10.1016/j.advwatres.2010.12.009.

DeChant, C. M., and H. Moradkhani (2012), Examining the effectiveness and robustness of sequential data assimilation methods for quantification of uncertainty in hydrologic forecasting, *Water Resour. Res.*, *48*, W04518, doi:10.1029/2011WR011011.

Dechant, C. M., and H. Moradkhani (2014), *Hydrologic Prediction and Uncertainty Quantification*, 387–414 pp., Taylor and Francis, Boca Raton, Fla.

Dee, D. P., and A. M. Da Silva (1998), Data assimilation in the presence of forecast bias, *Q. J. R. Meteorol. Soc.*, *124*(545), 269–295, doi:10.1002/qj.49712454512.

Dong, J., S. C. Steele-Dunne, T. E. Ochsner, and N. van de Giesen (2015a), Determining soil moisture by assimilating soil temperature measurements using the ensemble Kalman filter, *Adv. Water Resour.*, *86*, 340–353, doi:10.1016/j.advwatres.2015.08.011.

Dong, J., S. C. Steele-Dunne, J. Judge, and N. van de Giesen (2015b), A particle batch smoother for soil moisture estimation using soil temperature observations, *Adv. Water Resour.*, *83*, 111–122, doi:10.1016/j.advwatres.2015.05.017.

Dong, J., S. C. Steele-Dunne, T. E. Ochsner, and N. van de Giesen (2016a), Estimating soil moisture and soil thermal and hydraulic properties by assimilating soil temperatures using a particle batch smoother, *Adv. Water Resour.*, *91*, 104–116, doi:10.1016/j.advwatres.2016.03.008.
Dong, J., S. C. Steele-Dunne, T. E. Ochsner, and N. van de Giesen (2016b), Determining soil moisture and soil properties in vegetated areas by assimilating soil temperatures, *Water Resour. Res.*, *52*, 4280–4300, doi:10.1002/2015WR018425.
Doucet, A., and A. M. Johansen (2009), A tutorial on particle filtering and smoothing: Fifteen years later, in *Handbook of Nonlinear Filtering*, vol. 12, pp. 656–704, N. Y.
Dunne, S., and D. Entekhabi (2005), An ensemble-based reanalysis approach to land data assimilation, *Water Resour. Res.*, *41*, W02013, doi:10.1029/2004WR003449.
Evensen, G. (2003), The ensemble Kalman filter: Theoretical formulation and practical implementation, *Ocean Dyn.*, *53*(4), 343–367, doi:10.1007/s10236-003-0036-9.
Famiglietti, J., J. Rudnicki, and M. Rodell (1998), Variability in surface moisture content along a hillslope transect: Rattlesnake hill, Texas, *J. Hydrol.*, *210*(1), 259–281, doi:10.1016/S0022-1694(98)00187-5.
Famiglietti, J. S., D. Ryu, A. A. Berg, M. Rodell, and T. J. Jackson (2008), Field observations of soil moisture variability across scales, *Water Resour. Res.*, *44*, W01423, doi:10.1029/2006WR005804.
Fuhlendorf, S., and D. Engle (2004), Application of the fire–grazing interaction to restore a shifting mosaic on tallgrass prairie, *J. Appl. Ecol.*, *41*(4), 604–614, doi:10.1111/j.0021-8901.2004.00937.x.
Han, X., H.-J. H. Franssen, C. Montzka, and H. Vereecken (2014), Soil moisture and soil properties estimation in the Community Land Model with synthetic brightness temperature observations, *Water Resour. Res.*, *50*, 6081–6105, doi:10.1002/2013WR014586.
Hazenberg, P., Y. Fang, P. Broxton, D. Gochis, G.-Y. Niu, J. Pelletier, P. A. Troch, and X. Zeng (2015), A hybrid-3d hillslope hydrological model for use in earth system models, *Water Resour. Res.*, *51*, 8218–8239, doi:10.1002/2014WR016842.
Kim, G., and A. P. Barros (2002), Downscaling of remotely sensed soil moisture with a modified fractal interpolation method using contraction mapping and ancillary data, *Remote Sens. Environ.*, *83*(3), 400–413, doi:10.1016/S0034-4257(02)00044-5.
Koster, R. D., M. J. Suarez, R. W. Higgins, and H. M. Van den Dool (2003), Observational evidence that soil moisture variations affect precipitation, *Geophys. Res. Lett.*, *30*(5), 1241, doi:10.1029/2002GL016571.
Koster, R. D., S. P. P. Mahanama, B. Livneh, D. P. Lettenmaier, and R. H. Reichle (2010), Skill in streamflow forecasts derived from large-scale estimates of soil moisture and snow, *Nat. Geosci.*, *3*(9), 613–616, doi:10.1038/ngeo944.
Larson, K. M., E. E. Small, E. D. Gutmann, A. L. Bilich, J. J. Braun, and V. U. Zavorotny (2008), Use of GPS receivers as a soil moisture network for water cycle studies, *Geophys. Res. Lett.*, *35*, L24405, doi:10.1029/2008GL036013.
Lu, S., T. Ren, Y. Gong, and R. Horton (2007), An improved model for predicting soil thermal conductivity from water content at room temperature, *Soil Sci. Soc. Am. J.*, *71*(1), 8–14, doi:10.2136/sssaj2006.0041.
Madadgar, S., and H. Moradkhani (2014), Improved Bayesian multimodeling: Integration of copulas and Bayesian model averaging, *Water Resour. Res.*, *50*, 9586–9603, doi:10.1002/2014WR015965.
Margulis, S., M. Girotto, G. Cortes, and M. Durand (2015), A particle batch smoother approach to snow water equivalent estimation a particle batch smoother approach to snow water equivalent estimation, *J. Hydrometeorol.*, *16*, 1752–1772, doi:10.1175/JHM-D-14-0177.1.
McPherson, R. A., et al. (2007), Statewide monitoring of the mesoscale environment: A technical update on the Oklahoma Mesonet, *J. Atmos. Oceanic Technol.*, *24*(3), 301–321, doi:10.1175/JTECH1976.1.
Monsivais-Huertero, A., J. Judge, S. Steele-Dunne, and P.-W. Liu (2016), Impact of bias correction methods on estimation of soil moisture when assimilating active and passive microwave observations, *IEEE Trans. Geosci. Remote Sens.*, *54*(1), 262–278, doi:10.1109/TGRS.2015.2455037.
Montzka, C., H. Moradkhani, L. Weihermüller, H.-J. H. Franssen, M. Canty, and H. Vereecken (2011), Hydraulic parameter estimation by remotely-sensed top soil moisture observations with the particle filter, *J. Hydrol.*, *399*(3-4), 410–421, doi:10.1016/j.jhydrol.2011.01.020.
Moradkhani, H., K.-L. Hsu, H. Gupta, and S. Sorooshian (2005a), Uncertainty assessment of hydrologic model states and parameters: Sequential data assimilation using the particle filter, *Water Resour. Res.*, *41*, W05012, doi:10.1029/2004WR003604.
Moradkhani, H., S. Sorooshian, H. V. Gupta, and P. R. Houser (2005b), Dual state parameter estimation of hydrological models using ensemble Kalman filter, *Adv. Water Resour.*, *28*(2), 135–147, doi:10.1016/j.advwatres.2004.09.002.
Moradkhani, H., C. M. DeChant, and S. Sorooshian (2012), Evolution of ensemble data assimilation for uncertainty quantification using the particle filter-Markov chain Monte Carlo method, *Water Resour. Res.*, *48*, W12520 doi:10.1029/2012WR012144.
Niu, G.-Y., C. Paniconi, P. A. Troch, R. L. Scott, M. Durcik, X. Zeng, T. Huxman, and D. C. Goodrich (2014), An integrated modelling framework of catchment-scale ecohydrological processes: 1. model description and tests over an energy-limited watershed, *Ecohydrology*, *7*(2), 427–439, doi:10.1002/eco.1362.
Ochsner, T. E., M. H. Cosh, R. H. Cuenca, W. A. Dorigo, C. S. Draper, Y. Hagimoto, Y. H. Kerr, E. G. Njoku, E. E. Small, and M. Zreda (2013), State of the art in large-scale soil moisture monitoring, *Soil Sci. Soc. Am. J.*, *77*(6), 1888–1919, doi:10.2136/sssaj2013.03.0093.
Oleson, K. W., et al. (2010), *Technical Description of Version 4.0 of the Community Land Model (CLM)*, NCAR Technical Note NCAR/TN-478+STR, National Center for Atmospheric Research, Boulder, Colo., doi:10.5065/D6FB50WZ.
Peng, J., J. Niesel, and A. Loew (2015), Evaluation of soil moisture downscaling using a simple thermal-based proxy-the REMEDHUS network (Spain) example, *Hydrol. Earth Syst. Sci.*, *19*(12), 4765–4782, doi:10.5194/hess-19-4765-2015.
Piles, M., A. Camps, M. Vall-Llossera, I. Corbella, R. Panciera, C. Rudiger, Y. H. Kerr, and J. Walker (2011), Downscaling SMOS-derived soil moisture using MODIS visible/infrared data, *IEEE Trans. Geosci. Remote Sens.*, *49*(9), 3156–3166, doi:10.1109/TGRS.2011.2120615.
Ryu, D., W. T. Crow, X. Zhan, and T. J. Jackson (2009), Correcting unintended perturbation biases in hydrologic data assimilation, *J. Hydrometeorol.*, *10*(3), 734–750, doi:10.1175/2008JHM1038.1.
Sawada, Y., T. Koike, and J. P. Walker (2015), A land data assimilation system for simultaneous simulation of soil moisture and vegetation dynamics, *J. Geophys. Res. Atmos.*, *120*, 5910–5930, doi:10.1002/2014JD022895.
Sayde, C., C. Gregory, M. Gil-Rodriguez, N. Tufillaro, S. Tyler, N. van de Giesen, M. English, R. Cuenca, and J. S. Selker (2010), Feasibility of soil moisture monitoring with heated fiber optics, *Water Resour. Res.*, *46*, W06201, doi:10.1029/2009WR007846.
Sayde, C., J. B. Buelga, L. Rodriguez-Sinobas, L. El Khoury, M. English, N. van de Giesen, and J. S. Selker (2014), Mapping variability of soil water content and flux across 1–1000 m scales using the actively heated fiber optic method, *Water Resour. Res.*, *50*, 7302–7317, doi:10.1002/2013WR014983.
Selker, J. S., L. Thévenaz, H. Huwald, A. Mallet, W. Luxemburg, N. van De Giesen, M. Stejskal, J. Zeman, M. Westhoff, and M. B. Parlange (2006), Distributed fiber-optic temperature sensing for hydrologic systems, *Water Resour. Res.*, *42*, W12202, doi:10.1029/2006WR005326.
Seneviratne, S. I., T. Corti, E. L. Davin, M. Hirschi, E. B. Jaeger, I. Lehner, B. Orlowsky, and A. J. Teuling (2010), Investigating soil moisture-climate interactions in a changing climate: A review, *Earth Sci. Rev.*, *99*(3), 125–161, doi:10.1016/j.earscirev.2010.02.004.

Simunek, J., M. Sejna, H. Saito, M. Sakai, and M. T. Van Genuchten (2009), *The HYDRUS-1D Software Package for Simulating the One-Dimensional Movement of Water, Heat, and Multiple Solutes in Variably-Saturated Media*, Univ. of Calif., Riverside.

Sourbeer, J. J., and S. P. Loheide (2015), Obstacles to long-term soil moisture monitoring with heated distributed temperature sensing, *Hydrol. Processes*, doi:10.1002/hyp.10615.

Steele-Dunne, S. C., M. M. Rutten, D. M. Krzeminska, M. Hausner, S. W. Tyler, J. Selker, T. A. Bogaard, and N. C. van de Giesen (2010), Feasibility of soil moisture estimation using passive distributed temperature sensing, *Water Resour. Res.*, *46*, W03534, doi:10.1029/2009WR008272.

Striegl, A. M., S. P. Loheide, and S. P. Loheide II (2012), Heated distributed temperature sensing for field scale soil moisture monitoring, *Ground Water*, *50*(3), 340–347, doi:10.1111/j.1745-6584.2012.00928.x.

Su, H., Z.-L. Yang, G.-Y. Niu, and C. R. Wilson (2011), Parameter estimation in ensemble based snow data assimilation: A synthetic study, *Adv. Water Resour.*, *34*(3), 407–416, doi:10.1016/j.advwatres.2010.12.002.

Taylor, C. M., R. A. M. de Jeu, F. Guichard, P. P. Harris, and W. A. Dorigo (2012), Afternoon rain more likely over drier soils, *Nature*, *489*(7416), 423–426, doi:10.1038/nature11377.

Thyer, M., B. Renard, D. Kavetski, G. Kuczera, S. W. Franks, and S. Srikanthan (2009), Critical evaluation of parameter consistency and predictive uncertainty in hydrological modeling: A case study using Bayesian total error analysis, *Water Resour. Res.*, *45*, W00B14, doi:10.1029/2008WR006825.

van de Giesen, N., S. C. Steele-Dunne, J. Jansen, O. Hoes, M. B. Hausner, S. Tyler, and J. Selker (2012), Double-ended calibration of fiber-optic Raman spectra distributed temperature sensing data, *Sensors*, *12*(5), 5471–5485, doi:10.3390/s120505471.

Van Leeuwen, P. J., and G. Evensen (1996), Data assimilation and inverse methods in terms of a probabilistic formulation, *Mon. Weather Rev.*, *124*(12), 2898–2913, doi:10.1175/1520-0493(1996)124 < 2898:DAAIMI>2.0.CO;2.

Vereecken, H., T. Kamai, T. Harter, R. Kasteel, J. Hopmans, and J. Vanderborght (2007), Explaining soil moisture variability as a function of mean soil moisture: A stochastic unsaturated flow perspective, *Geophys. Res. Lett.*, *34*, L22402, doi:10.1029/2007GL031813.

Wood, E. F., et al. (2011), Hyperresolution global land surface modeling: Meeting a grand challenge for monitoring earth's terrestrial water, *Water Resour. Res.*, *47*, W05301, doi:10.1029/2010WR010090.

Yan, H., C. M. DeChant, and H. Moradkhani (2015), Improving soil moisture profile prediction with the particle filter-Markov Chain Monte Carlo method, *IEEE Trans. Geosci. Remote Sens.*, *50*, 6134–6147, doi:10.1109/TGRS.2015.2432067.

Zreda, M., D. Desilets, T. Ferré, and R. L. Scott (2008), Measuring soil moisture content non-invasively at intermediate spatial scale using cosmic-ray neutrons, *Geophys. Res. Lett.*, *35*, L21402, doi:10.1029/2008GL035655.